Regulation of gene expression and chromatin structure by JIL-1 mediated histone H3 serine10 phosphorylation in *Drosophila*

by

Yeran Li

A dissertation submitted to the graduate faculty

in partial fulfillment of the requirements for the degree of

DOCTOR OF PHILOSOPHY

Major: Molecular, Cellular and Developmental Biology

Program of Study Committee:
Kristen M. Johansen, Major Professor
Jørgen Johansen
Jack Girton
Hui-Hsien Chou
Edward Yu

Iowa State University

Ames, Iowa

2015

TABLE OF CONTENTS

ABSTRACT iii

CHAPTER 1. GENERAL INTRODUCTION 1
Background 1
Research Questions And Significance 6
Thesis Organization 7
References 8

CHAPTER 2. LITERATURE REVIEW 11
Chromatin Structure and Organization 11
Chromatin Remodeling 15
Accelerating Biological Discoveries With Next-Generation Sequencing 23
References 25

CHAPTER 3. DOMAIN REQUIREMENTS OF THE JIL-1 TANDEM KINASE FOR HISTONE H3S10 PHOSPHORYLATION AND CHROMATIN REMODELING IN VIVO 35
Summary 35
Introduction 36
Experimental Procedures 37
Results 42
Discussion 49
References 52
Figures 56
Tables 62

CHAPTER 4. GENOME-WIDE ANALYSIS OF REGULATION OF GENE EXPRESSION AND H3K9me2 DISTRIBUTION BY JIL-1 KINASE MEDIATED HISTONE H3S10 PHOSPHORYLATION IN *DROSOPHILA* 63
Summary 63
Introduction 64
Materials And Methods 66
Results 71
Discussion 80
Acknowledgements 84
References 84
Figures 89
Supplemental Materials 97

CHAPTER 5. GENERAL CONCLUSION 100
General Discussion And Future Directions 100
References 103

ACKNOWLEDGEMENTS 104

ABSTRACT

Epigenetic processes, such as histone modifications, play essential roles in regulating chromatin structure and gene expression. In *Drosophila JIL*-1 tandem kinase has been identified as a major regulator of chromatin structure and gene expression. It has been demonstrated that JIL-1 is responsible for histone H3 serine 10 (H3S10) phosphorylation at interphase, which counteracts gene silencing marker histone H3 lysine 9 (H3K9) dimethylation. In addition, JIL-1 localizes specifically to euchromatic interband regions, and a reduction in JIL-1 levels lead to a global disruption of chromatin morphology.

JIL-1 can be divided into four domains, including an NH_2- terminal domain (NTD), two kinase domains (KDI and KDII), and a COOH-terminal domain (CTD). Functions of all four domains have been characterized. The NTD is essential for JIL-1 kinase activity; a truncated JIL-1 protein without the NTD fails to phosphorylate H3S10 despite its proper localization on the chromosome and the presence of both kinase domains. Both kinase domains are required for JIL-1's kinase activity and have equal importance. The CTD is sufficient for JIL's localization to chromosome, but not required for kinase activity.

Furthermore, to explore the mechanisms of JIL-1 mediated histone modification and its interplay with other histone markers, we have conducted a genome-wide study of relationships between JIL-1 mediated H3S10 phosphorylation and H3K9 dimethylation in binding profiles and gene expression. Utilizing ChIP-seq, we show that the H3S10 phosphorylation marker is localized

predominantly to active genes, whereas the silencing H3K9 dimethylation marker is enriched at inactive genes. Additionally, studying the transcription profile using RNA-seq reveals functions of JIL-1 in maintaining a balance between active and inactive transcribed genes, where down-regulation of genes in the *JIL-1* mutant is associated with elevated levels of H3K9 dimethylation, whereas up-regulation of genes is correlated with loss of H3K9 dimethylation. These results support a model where gene expression levels are regulated by H3K9 dimethylation independent of the state of H3S10 phosphorylation, which in turn functions to indirectly maintain active transcription by counteracting H3K9 dimethylation.

CHAPTER 1. GENERAL INTRODUCTION

Background

In eukaryotes chromatin is a complex of macromolecules consisting of DNA and histone protein, whose essential function is to package DNA into a small volume to fit within cells. However, various DNA machineries require access to compacted DNA to accomplish their tasks, such as gene transcription, DNA replication, and mitosis. The solution to such issues is to allow a dynamic change in chromatin structure and organization. So far, there are three mechanisms that have been studied: ATP dependent chromatin remodeling, histone exchange, and histone modification (Baker and Grant, 2007; Henikoff, 2008).

ATP dependent remodeling utilizes the energy of ATP hydrolysis to locally alter the association of histones with DNA (Vignali et al., 2000). Histone exchange is the process in which common histones are replaced by their variants, which affects nucleosome stability and can recruit remodeling factors (Jin et al., 2005). Additionally, covalent modification on histone N-terminal tails can alter chromatin structure by addition or removal of various chemical residues. By utilizing specific antibodies and mass spectrometry, a number of histone modifications have been identified: acetylation, methylation, phosphorylation, ubiquitylation among others (Kouzarides, 2007; Stanley et al., 2001). The mechanisms underlying histone modification include disruption of contacts between nucleosomes to unwrap compacted chromatin, and

recruitment of non-histone proteins with enzymatic activities (Kouzarides, 2007). Different histone modifications can work in a combinational manner that has been termed a “histone code”, which extends the information potential (Jenuwein and Allis, 2001).

Histone H3 Serine10 (H3S10) phosphorylation is among the most important histone modifications due to its versatile functions within cells. H3S10 phosphorylation appears to have two contradictory functions at different stages of the cell cycle: 1) During metaphase, it facilitates chromosome condensation and segregation; 2) During interphase it promotes chromatin decondensation and transcription activation (Hendzel et al., 1997; Wei et al., 1999; Sassone-Corsi et al., 1999). One of the explanations for this paradox is that H3S10 phosphorylation may take action with diverse histone modifications varying stages of a cell cycle (Strahl and Allis, 2000).

As a tandem kinase JIL-1 was first identified through an expression library screening with antibody mAb2A (Johansen et al., 1996). JIL-1 is 134 kDa in size and can be divided into four domains including an N-terminal domain (NTD), kinase domain I (KDI), kinase domain (KDII), and the C-terminal domain (CTD). Human MSK and *Drosophila* RSK share homology to JIL-1 (Jin et al., 1999). The function of MSK is to activate transcription by 1) phosphorylation of transcription factors (Deak et al., 1998) and 2) phosphorylation of histone H3S10, a active transcriptional marker (Ito, 2007; Kouzarides, 2007). However, JIL-1 has extra NTD and CTD domains compared to MSK, which indicates more complex functions of JIL-1.

JIL-1 is an essential protein for many developmental stages. Animals without JIL-1 protein cannot survive to adulthood. *Drosophila* larvae are viable but their polytene chromosome structure is tremendously coiled and disrupted, which is especially apparent with the male X chromosome (Wang et al., 2001). Also, smaller ovaries and abnormal egg-chambers are observed in animals with low JIL-1 expression (Zhang et al., 2003).

It has been demonstrated that JIL-1 is a histone H3S10 kinase and undergoes auto-phosphorylation through *in vitro* kinase assays (Jin et al., 1999). In the *JIL-1* null mutant where there is no JIL-1 expression, H3S10 phosphorylation levels are significantly decreased as analyzed by immunostaining of polytene chromosome and immunoblotting. However, in cells undergoing mitosis H3S10 phosphorylation levels are unaltered in JIL-1 null mutant (Wang et al., 2001). These results indicate that JIL-1 is required for H3S10 phosphorylation in interphase but not metaphase.

JIL-1 localizes specifically to interband regions and the chromatin morphology is largely disrupted in JIL-1 null mutant, which implies it plays an important role in higher-order chromatin structure. Using a LacI tagged JIL-1 construct, Deng and colleagues specifically targeted JIL-1 to a band region containing LacI operator repeat. This ectopically expressed, active JIL-1 turned the local compacted region into a decondensed chromatin region, whereas an inactive "kinase dead" JIL-1 construct failed to do so. These results indicate that JIL-1 mediates H3S10 phosphorylation to maintain decondensed chromatin structure (Deng et al., 2008). JIL-1's unique

distribution also suggests that it is involved in active transcription, as majority of the active genes are located at interband regions. Other evidence supporting such a conclusion include JIL-1's enrichment on the male-X chromosome, where some dosage compensation models suggest genes need to be up regulated to compensate for the two X chromosomes in females (Jin et al., 2000).

JIL-1's ability to regulate higher-chromatin structure can also be reflected on a genome-wide scale, in which JIL-1 and its mediated H3S10 phosphorylation are capable of counteracting heterochromatic spreading and gene silencing (Wang et al., 2011). Chromatins in the nucleus of *Drosophila* can be broadly classified into two types: a lightly packed form called euchromatin and more tightly packed form called heterochromatin. Heterochromatic region includes chromocenter and telomere, and chromosome arms are mostly euchromatic region despite the existence of facultative heterochromatin associated with morphogenesis or differentiation. In the *JIL-1* null mutant, the heterochromatic marker H3K9me2 spreads from the chromocenter region to the chromosome arms, where H3S10 phosphorylation originally dominated. It has been shown that Su(var)3-9, the histone methyltransferase (HMT) catalyzing H3K9 methylation, genetically interacts with JIL-1. Additionally, the *Su(var)3-9* mutant is able to rescue the phenotype and viability of a *JIL-1* null mutant (Zhang et al., 2006). Similar conclusions have been drawn from various experiments such as position-effect variegation (PEV) assay and Next-generation sequencing (Wang et al.,

2011, Cai et al., 2014). These results suggest JIL-1 is involved in maintaining higher-order chromatin structure via regulating heterochromatin formation.

As described above, JIL-1 can be divided into four domains: NTD, KDI, KDII, and CTD. Bao and her colleagues demonstrated that the JIL-1 CTD is required for correct targeting on the polytene. Expression of JIL-1's CTD is able to rescue the viability and polytene chromosome morphology in a *JIL-1* null mutant animal. However, over-expression of JIL-1 CTD significantly decreases endogenous phosphorylated H3S10 levels, yet still results in normal chromosome morphology and low lethality (Bao et al., 2008). Compared with the CTD, the other domains are poorly studied. Data from this study also have shown that NTD plus both kinase domains together can increase the H3S10 kinase activity. This NTD-KDI-KDII combination rescues autosome chromosome morphology completely but leaves the morphology of male X chromosome partly restored. In addition although most of this truncated protein localizes to interbands as that in wild type, its distribution is broader. These results indicate that JIL-1 has a second mechanism for chromatin association. However, neither the NTD domain alone nor the tandem kinase domains alone could repeat these results (Bao et al., 2008). This collective data suggests that further study of the NTD and kinase domains will yield further clues into understanding JIL-1’s function and mechanisms.

Research Questions And Significance

What are the functions of JIL-1's N-terminal domain and two kinase domains?

JIl-1 is a tandem kinase consisting of four domains: NTD, KDI, KDII and CTD. The functions of the CTD have been well characterized but the roles of the others remain unclear. In order to dissect JIL-1's function throughout, it is necessary to understand the other domains. First, by utilizing a series of truncated JIL-1 constructs we have shown that the JIL-1 construct without the NTD is unable to phosphorylate H3S10 although it maintains a normal localization to polytene chromosomes. Second, we have demonstrated that both kinase domains are required for JIL-1's kinase activity. Additionally, this kinase activity is abolished when phosphorylation at Serine 424 is absent. Thus, this data supports a model where the NTD of JIL-1 is required for kinase activity by properly positioning the protein, and the activation of the first kinase domain is dependent on the phosphorylation of Serine 424.

Genome-wide, how does JIL-1 and its mediated H3S10 phosphorylation regulate gene expression via coordinating the distribution of the gene silencing mark?

With genetic interaction assays and position-effect variegation (PEV) assays, our laboratory has identified that the function of H3S10 phosphorylation is to antagonize heterochromatin formation by balancing active and inactive gene expression markers. However, these conclusions are drawn from a specific gene locus (*white* gene), an analysis at the genome-wide level is lacking. We performed Chromatin Immunoprecipitation coupled with deep sequencing (ChIP-seq) using antibodies against JIL-1, H3S10 phosphorylation, and H3K9

dimethylation, and used RNA-seq to examine the gene expression profiles from wild type and *JIL-1* mutants. The results have shown that H3S10 phosphorylation maintains active transcription by counteracting H3K9 dimethylation and gene silencing.

Thesis Organization

Chapter 1 summarizes the studies that have been done to understand the basic features of JIL-1 and the mechanisms behind its role in regulating chromatin organization and structure. Then two research questions regarding to JIL-1's domain functions and its genome-wide relationship with silencing marker are briefly discussed.

Chapter 2 is a literature review regarding chromatin structure, chromatin remodeling, histone modification, histone exchange, and next-generation sequencing technology.

Chapter 3 discusses the domain requirements for JIL-1 to achieve its normal kinase activity. Yeran Li made JIL-1-ΔNTD and JIL-1^{S425A} transgenic flies, analyzed the expression level of various JIL-1 truncated constructs, and studied the effect of JIL-1 Serine 424 (Fig.1, 3, 4, 6). Dr. Weili Cai generated JIL-1 CTD and JIL-1 ΔCTD transgenic flies, and discovered JIL-1's kinase activity was required for its ability to alter higher-order chromatin structure (Fig. 2, 3, 5). Dr. Xiaomin Bao contributed to JIL-1 kinase dead transgenic flies.

Chapter 4 details the genome-wide distribution of JIL-1, H3S10ph and H3K9me2, and expression profiles of wild type and *JIL-1* mutant cells from the

salivary gland. Dr. Weili Cai, Dr. Chao Wang and Yeran Li performed ChIP-seq and RNA-seq sample preparation, qPCR analysis and statistical and bioinformatic analysis of the next generation sequencing data. Dr. Sanzhen Liu contributed to data trimming, and Lu Shen provided statistical analysis expertise.

Chapter 5 covers the general conclusion of the JIL-1 project and future direction.

References

Baker SP, Grant PA. (2007). The SAGA continues: expanding the cellular role of a transcriptional co-activator complex. *Oncogene*. 26(37): 5329-40.

Bao X, Cai W, Deng H, Zhang W, Krencik R, Girton J, Johansen J and Johansen KM. (2008). The COOH-terminal domain of the JIL-1 histone H3S10 kinase interacts with histone H3 and is required for correct targeting to chromatin. *J Biol Chem*. 283:32741-32750.

Deak M, Clifton AD, Lucocq JM, Alessi DR. (1998). Mitogen- and stress-activated protein kinase-1 (MSK1) is directly activated by MAPK and SAPK2/p38, and may mediate activation of CREB. *EMBO J*. 17: 4426-41

Deng H, Bao X, Cai W, Blacketer MJ, Belmont AS, Girton J, Johansen J and Johansen KM. (2008). Ectopic histone H3S10 phosphorylation causes chromatin structure remodeling in *Drosophila*. *Development.* 135 : 699-705.

Hendzel MJ, Wei Y, Mancini MA, Van Hooser A, Ranalli T, Brinkley BR, Bazett-Jones DP and Allis CD. (1997). Mitosis-specific phosphorylation of histone H3 initiates primarily within pericentromeric heterochromatin during G2 and spreads in an ordered fashion coincident with mitotic chromosome condensation. *Chromosoma*.106(6):348-360.

Henikoff S. (2008). Nucleosome destabilization in the epigenetic regulation of gene expression. *Nat Rev Genet.* 9:15-26.

Ito T. (2007). Role of histone modification in chromatin dynamics. *J. Biochem*. 141: 609- 614

Jenuwein T, Allis CD. (2001). Translating the histone code. *Science.* 10;293(5532):1074-80.

Jin J, Cai Y, Li B, Conaway RC, Workman JL, Conaway JW, Kusch T. (2005). *Trends Biochem Sci*. 30(12):680-7.

Kouzarides T. (2007). Chromatin modifications and their function. *Cell.* 128:693-705.

Jin Y, Wang Y, Walker DL, Dong H, Conley C, Johansen J and Johansen KM. (1999). JIL-1: a novel chromosomal tandem kinase implicated in transcriptional regulation in *Drosophila*. *Mol Cell.* 4:129-135.

Jin, Y, Wang Y, Johansen J and Johansen KM. (2000). JIL-1, a chromosomal kinase implicated in regulation of chromatin structure, associates with the MSL dosage compensation complex. *J. Cell Biol.* 149 : 1005-1010.

Johansen KM. (1996). Dynamic remodeling of nuclear architecture during the cell cycle. *J Cell Biochem.* 60:289-296.

Sassone-Corsi P, Mizzen CA, Cheung P, Crosio C, Monaco L, Jacquot S, Hanauer A and Allis CD. (1999). Requirement of Rsk-2 for epidermal growth factor-activated phosphorylation of histone H3. *Science.* 285:886-891.

Stanley JS, Griffin JB, Zempleni J. (2001). Biotinylation of histones in human cells. Effects of cell proliferation. *Eur J Biochem*. 268(20):5424-9.

Strahl BD and Allis CD. (2000). The language of covalent histone modifications. *Nature.*403:41-45.

Vignali M, Hassan AH, Neely KE, Workman JL. (2000). ATP-Dependent Chromatin-Remodeling Complexes. *Mol Cell Biol.* 2000 Mar;20(6):1899-910.

Wang Y, Zhang W, Jin Y, Johansen J and Johansen KM. (2001). The JIL-1 tandem kinase mediates histone H3 phosphorylation and is required for maintenance of chromatin structure in *Drosophila*. *Cell* 105:433-443.

Wang C, Cai W, Deng H, Bao X, Girton J, Johansen J and Johansen KM. (2011). The epigenetic H3S10ph mark is required for counteracting heterochromatic spreading and gene silencing in *Drosophila*. *J. Cell Sci.* 124 : 4309-4317.

Wei Y, Yu L, Bowen J, Gorovsky MA and Allis CD. (1999). Phosphorylation of histone H3 is required for proper chromosome condensation and segregation. *Cell*. 97(1): 99-109.

Zhang W, Wang Y, Long J, Girton J, Johansen J and Johansen KM. (2003). A developmentally regulated splice variant from the complex lola locus

encoding multiple different zinc-finger domain proteins interacts with the chromosomal kinase JIL-1. *J. Biol. Chem.* 278 : 11696-11704.

Zhang W, Deng H, Bao X, Lerach S, Girton J, Johansen J and Johansen KM. (2006). The JIL-1 histone H3S10 kinase regulates dimethyl histone H3K9 modifications and heterochromatic spreading in *Drosophila*. *Development* 133 : 229-235.

CHAPTER 2. LITERATURE REVIEW

Chromatin Structure And Organization

Chromatin is a compact form of DNA in eukaryotic cells, consisting of DNA and proteins. Nucleosomes are the fundamental unit of chromatin, which contains 147bp DNA wrapped around an octamer of 4 core histones, containing one H3-H4 tetramer and two H2A-H2B dimers (Kornberg, 1974, Arents et al., 1991; Richmond et al., 1993; Luger et al., 1997). The C-terminal histone-fold domains of core histones are conserved, consisting of a "helix turn helix turn helix" motif. This conformation is critical for assembly of nucleosome via facilitating histone-DNA and histone-histone interaction (Luger et al., 1997; Wolffe, 1998). The N-terminal domain of core histones (histone tail) is flexible and less structured, which is thought to act as a platform to make contact with DNA and adjacent nucleosomes. Especially the N-terminal tails of histones H3 and H4 protrude from the nucleosome and are subjected to diverse modifications such as phosphorylation, methylation and acetylation (Luger et al., 1997). Modifications can also occur to histone H2A and H2B, but are less common.

The nucleosome array, a “beads-on-string” fiber with diameter of 11 nm, characterizes the first level of chromatin organization (Luger et al., 1997). The binding of histone H1 to DNA outside each nucleosome core organizes the nucleosome array into a helix of nucleosomes with a diameter of about 30 nm and a packing density of about 6 to 7 nucleosomes per 11 nm (Song et al., 2014). Earlier studies of chromatin organization have led to two models for the

30 nm fiber: 1) arranged linearly in a one-start solenoid-type helix with bent liner DNA, or 2) organized to zigzag back and forth in a two-start stack of nucleosomes connected by a relatively straight DNA linker (Finch et al., 1976; Woodcock et al., 1984; Williams et al., 1986). The latter class can be further divided into the twisted crossed-linked model and the helical ribbon model based on the differences in the orientation angles between the linker DNA and fiber axes (Woodcock et al., 1984; Williams et al., 1986; Smith et al., 1990). Recently, Song and his colleagues revealed that the 30 nm fiber was packaged in two interwound left-handed helical stacks with a straight linker DNA between successive nucleosomes in the array crossing the interior of the fiber via cryo-electron microscopy (Song et al., 2014).

The metaphase chromosome, in which DNA is compacted 10,000 to 20,000 folds, represents the most obvious chromatin higher-order structure. Due to its complexity, its structure beyond the 30 nm fiber remains largely uncharacterized. The general conclusion from decades of study indicates that mitotic chromosomes consist of a network or gel where individual chromatin fibers are connected by crosslinking elements (Poirier and Marko, 2002).

Polytene chromosomes in *Drosophila*

An over-sized chromosome, the polytene chromosome ("multi-stranded"), is considered to be useful for studying interphase chromosome organization. It was first discovered in the salivary gland of *Chironomus* but was later studied in *Drosophila.* It develops from chromosomes of diploid nuclei by duplication of the normal chromosome. However, chromosomes do not segregate at the end of each S-phase but remain paired to each other,

eventually after many rounds of replication forming polytene chromosomes with 1024 copies of each chromatid (Zhimulev, 1996). Due to this special duplication feature, polytene chromosomes are much larger than regular diploid chromosomes, which make them easily observed under a common microscope. Using microscopy, polytene chromosomes are noticeable for their banding pattern comprised of intervals of band and interband, depending on the composition of chromatin material. General conclusions have been made regarding the banding pattern of polytene chromosomes: bands are highly packed and therefore are more dense, and harbor inactivated genes; in contrast, interbands are lightly packed with less dense, and are characterized by their association with active genes (Speiser, 1974; Zhimulev and Belyaeva, 1975; Zhimulev et al., 2014).

Euchromatin and heterochromatin

The interphase chromatin can also be classified into heterochromatin and euchromatin with regard to states of compaction and transcriptional potential. Chromosome arms are generally considered euchromatin, where it is gene rich, less condensed and associated with active gene transcription. In contrast, heterochromatin is found mostly at the chromocenter and telomeres, and is generally gene poor, highly condensed, and associated with repression of gene transcription (Wang et al., 2014). Heterochromatin can be further classified into two categories: constitutive and facultative heterochromatin. Constitutive heterochromatin is always compact and is comprised of repetitive DNA sequences, whereas facultative heterochromatin can transform from a compact, transcriptionally inactive state into an open and transcriptionally

active state depending on the environment (Trojer and Reinberg, 2007). These events are generally accomplished by changes in histone modifications and histone variants (Liaw and Lustig 2006; Hines et al., 2009).

Heterochromatin and euchromatin are both critical for maintaining the genome integrity, but heterochromatin is able to spread to neighboring euchromatic regions and regulate gene expression. Using position-effect variegation (PEV) in *Drosophila,* studies have discovered the role of heterochromatin in transcription regulation. The *white* gene, which is responsible for the presence of the red pigment in *Drosophila* eyes, is located at the euchromatic region. However, when a heterochromatin region is ectopically placed flanking the *white* gene, *white* expression is variably silenced. The different expression states of the *white* gene result in mosaic eyes with red and white pigmentation (Elgin and Reuter, 2007). As introduced in the next section, it is well recognized that chromatin structure is regulated by histone modification and chromatin remodeling activities (Zentner and Henikoff, 2013). Heterochromatin assembly and spreading largely depend on these two factors, as heterochromatic regions are often associated with specific gene silencing markers such as histone methylation. Histone methylation can indirectly affects chromatin structure by 1) antagonizing euchromatic markers, such as phosphorylation and acetylation (Pasini et al., 2010; Zhang et al., 2006); and 2) serving as a docking site for the recruitment of heterochromatin-assembly protein, such as HP1 and Su(var)3-9 (Nakayama et al., 2001; Lachner et al., 2001).

Chromatin Remodeling

As discussed in the previous section, chromatin has a very compact structure, packaging more than 2 m of the genome in a nucleus with a diameter of 10 μm (Yaniv, 2014). The nature of this assembly is a significant barrier for enzymes requiring DNA access, which is critical for cellular functions such as DNA replication, DNA repair, and transcription. To tackle this issue, chromatin has utilizes three strategies to maintain its stability and integrate but also disrupt its condensation dynamically: 1) histone modification; 2) histone variants exchange; and 3) ATP-dependent chromatin remodeling (Baker and Grant, 2007; Henikoff, 2008).

Histone modification

The majority of covalent modifications take place at the N-terminal domains (histone tail) of all core histones. These domains are exposed to the nucleosome surface and do not directly participate in the nucleosome integrity. However, the N-terminal tails provide platforms for chromatin remodeling proteins and other functional groups to bind to chromatin. For example, acetylated lysine can be recognized by ATP-dependent remodeling enzymes containing Bromo-domains (Owen et al., 2000). Additionally, the covalent modification itself can directly disrupt the DNA-histone interactions. For example, acetylation of lysine neutralizes its positive change, which causes the acetylated nucleosomes less functionality in repelling negatively charged DNA (Tse et al., 1998). There are over one hundred distinct modifications

described in the literature, and common modifications include lysine methylation (Kme), serine phosphorylation (Sph), lysine acetylation (Kac), and ADP-ribosylation (ar) (Rando, 2012; Turner, 2005; Kouzarides, 2007). They are involved in versatile biological events such as maintaining higher-order chromatin organization and regulating transcription activity (Shogren-Knaak et al., 2006; Wolffe and Hayes, 1999; Cheung et al., 2000).

Histone phosphorylation

All four histone tails with acceptor sites can be phosphorylated by kinases and de-phosphorylated by phosphatases. Histone phosphorylation can occur on serine, threonine and tyrosine residues. A series of kinases have been studied in the past two decades. The mammalian MSK1/2 kinase, RSK, ,yeast SNF1 and *Drosophila* JIL-1 have been found to be kinases of H3S10 (Kouzarides, 2007; Sassone-Corsi et al., 1999; Jin et al., 1999), and the mammalian Aurora B is responsible for H3S10 and H3S28 phosphorylation (Goto et al., 2002).

Histone phosphorylation is highly conserved in yeast and humans, implying its importance in various biological events such as regulating chromatin compaction, transcription regulation, and DNA damage repair. Regarding chromatin condensation, phosphorylation of H3S10 has been a well-studied marker. Interestingly, studies have unveiled two contradictory functions of this modification: during interphase H3S10 phosphorylation is found associated with loosely packed chromatin and active gene transcription (Strelkov and Davie, 2002; Sassone-Corsi et al., 1999); however, during mitosis it is enriched in mitotic compacted chromosomes, which indicates a

function in chromosome condensation (Wei et al., 1999). The contradictory functions most likely are caused by the combination of different histone modifications.

A great number of histone phosphorylation events are associated with active gene expression. In *Drosophila the* H3S10 phosphorylation marker is enriched at interband regions on polytene chromosomes where actively transcribed genes are located (Wang et al., 2001, Cai et al., 2014). In mammals, H3S10 and H2BS32 phosphorylation have been associated with regulation of epidermal growth factor (EGF)-response gene transcription (Lau et al., 2011; Chadee et al., 1999). Mechanically, H3S10, H3S28, and H3T11 phosphorylation are found associated with another active transcription marker, H3 acetylation, strongly implying a role in active gene expression (Rossetto et al., 2012).

Histone acetylation

Histone acetylation is applied and removed by two families of enzymes: histone acetyl-transferases (HATs) and histone deacetylases (HDACs) (Xhemalce et al., 2011). HATs transfer acetyl-groups to lysines from acetyl-CoA. By doing so, the additional acetyl-group neutralizes lysine's positive charge and this reaction has the potential to reduce the interaction between DNA and histone. There are three types of HATs in the nucleus depending on amino-acid sequence homology and conformation structure: GNAT, MYST and CBP/p300 families (Hodawadekar et al., 2007).

Histone acetylation is mainly associated with transcription activation due to its chemical property (Allfrey et al., 1964). For example, H4K16 acetylation

is up-regulated at the male X chromosome in *Drosophila,* where the prevailing model posits that gene expression needs to be doubled to compensate products from two copies of X chromosomes in females (Hilfiker et al., 1997; Akhtar et al., 2000).

HDACs reverse the effects of HATs by removing acetyl-group from lysines. They stabilize and tighten the local chromatin organization, and serve as transcriptional silencing markers. In yeast and mammals, four types of HDACs (HDAC I, II, III, X) have been identified based on sequence similarity (Gray and Ekstrom, 2001; Yang et al., 2008). Studies have shown that members from HDAC I and III are able to deacetylate histone H4 (Barlow et al., 2001). Additionally, knockdown of individual HDACs in S2 cells demonstrates HDAC I and III is able to affect gene expression (Foglietti et al., 2006). However, in one experiment an over-expression of RPD3, one of the HDAC Is, led to gene up-regulation (Swaminathan, 2012). Also, recent studies suggest H3K9 methylation and HP1 mediated heterochromatin formation demand H4K12 acetylation (Swaminathan et al., 2005; Zhou et al., 2011). Although most acetylation is associated with active gene transcription, these results suggest that acetylation may have many complex roles.

Histone methylation

Histone methylation can occur on arginine, lysine and histidine (Strahl and Allis, 2000; Tan et al., 2011; Byvoet et al., 1972). Different from acetylation and phosphorylation, lysine can be mono-methylated (me1), di-methylated (me2) and tri-methylated (me3) (Murray, 1964; Paik and Kim, 1967; Haempel et al., 1968). The most studied methylation includes H3

lysine4 (H3K4), H3K9 and H3K27. Histone methylation is a reversible process and histones can be methylated and de-methylated by histone methyl-transferases (HMTs) and demethylases. Three families of HMTs have been identified based on their sequence similarity: SET-domain containing proteins, DOT1-like proteins, and protein arginine N-methyltransferase (PRMT) (Rea et al., 2000; Feng et al., 2002; Bannister and Kouzarides, 2011). There are two families of demethylases for demethylate methyl-lysines that are highly conserved from yeast to human: amine oxidases and jumonji C (JmjC)-domain-containing, iron-dependent dioxygenases (Shi et al., 2004, Tsukada et al., 2006; Whetstine et al., 2006; Cloos et al., 2006).

Unlike histone acetylation, histone methylation contributes greater complexity to biological events, and these effects are mostly context-dependent. Different degrees of methylation have been associated with various gene expression statuses. For example, H3K9me2 is associated with gene silencing, whereas H3K4me3 is generally accompanied with active transcription (Bernstein et al., 2002). Combining different histone methylation markers can lead to different effects compared with appearing alone. Although H3K4me3 and H3K27me3 are marks associated with active and inactive gene expression respectively, when they interact together they appear to compromise their functionalities. By doing so, genes at regions containing both marks remain transcriptionally silenced, but are kept poised for activation (Bernstein et al., 2006).

Cross-talk among histones

As discussed before, each histone modification has its unique function. However, histone modification is not an isolated event; but tworks together in combination: a modification may facilitate or repress the behavior of flanking modifications (Jenuwein and Allis, 2001). In mammalian cells, the H4K16 acetylation can be enhanced by H3S10 phosphorylation by interacting with other proteins that bind to H3S10 and H4K16 separately (Zippo et al., 2009). Another example is that HP1, which binds to methylated H3K9, fails to do so when H3S10 is phosphorylated (Fischle et al., 2005; Mateescu et al., 2008). The combination of differing histone modifications show an elegant regulation of various biological events, but as such, also makes it hard to reveal the mechanisms behind it.

Histone variants and histone exchanges

As briefly mentioned in the earlier section, histone exchange is one of the mechanisms to remodel chromatin structure by deploying histone variants. Histone variants are non-allelic variants of canonical histones, and differ from their canonical counterparts in primary sequence and expression timing (Kamakaka and Biggins, 2005; Ausio and Abbott, 2002). Unlike canonical core histones expressed only during S phase with multiple-copy genes, histone variants are usually transcribed from single-copy genes throughout the cell cycle (Marzluff et al., 2008). These diversities lead to changes in physical properties and the way they are incorporated into chromatin, thereby altering chromatin structure and organization. Histone variants can be assembled and disassembled from the nucleosome by histone chaperones through physical

interactions. Studies have found that histone chaperones are critical in complete eviction of nucleosomes at promoter regions in yeast (Lee et al., 2004). Because histone chaperones have dissimilar relative affinities for different variants, chaperone-histone interactions are highly specific (Park and Luger, 2008).

Due to the complexity of histone interactions, histone variants have undergone different degrees of evolvement from core histones under various structural requirements (Talbert and Henikoff, 2010; Malik and Henikoff, 2003). For example, H4 is the slowest evolving core histone, with no variant found in higher eukaryotic animals (Malik and Henikoff, 2003). On the contrary, H2A has the largest number of variants, and this is probably due to its peripheral location and its frequent interaction with other histones (Bonisch and Hake, 2012). The H2A variant family includes H2A.Z, H2A, X, MacroH2A, H2A-Bbd, and H2Av (Ausio and Abbott 2002; Redon et al. 2002; Fernandez-Capetillo et al. 2004). H2A.X and H2A.Z are conserved from yeast and human, while others such as H2A-Bbd, are restricted to vertebrates (Chadwick and Willard 2001). The H2A variants are different from the canonical histones by their C-terminal tails in both length and sequence, including the docking domain, L1 loop and acidic patch. For example, an H2A.Z nucleosome fails to form hydrogen bonds between its docking domain and H3 compared with its canonical counterpart, resulting in subtle nucleosome destabilization (Weber et al. 2010).

H2Av in *Drosophila*

In *Drosophila* there is only one H2A variant, H2Av, whose sequence contains features from both H2A.X and H2A.Z (Talbert PB et al., 2002). Compared to sequences of other H2A variants, it clearly indicates that H2Av belongs to the H2A.Z family (Malik and Henikoff 2003; Talbert and Henikoff, 2010). However, the C-terminus of H2Av contains amino acids SQAY, which is similar to SQ[E/D]Φ motif found in H2A.X. Thus, H2Av appears to respond to DNA damage as H2A.X and regulate transcription as H2A.Z in *Drosophila*. H2Av also has its distinct functions such as assembly of heterochromatin in *Drosophila* (Swaminathan et al., 2005). H2Av has a wide but not uniform distribution on both euchromatic and heterochromatic regions of polytene chromosome with higher enrichment at the end of the chromosome (Leach et al., 2000; Zhang and Pugh 2011). Chromatin immunoprecipitation (ChIP) combined with qPCR has shown that H2Av has similar enrichment at both actively and inactively transcribed genes. However, the level of H2Av is largely reduced at the heat-shock induced open chromatin region (Leach et al., 2000). Similarly, H2A.Z is depleted from highly transcribed chromatin in human cells (Hardy et al., 2009). Genome-wide analysis provides detailed mapping of H2Av, which sheds light on understanding its functions. H2Av containing nucleosomes are enriched downstream of the transcription start site (TSS) with a 175 base pair interval in *Drosophila,* and this occupancy is decreased as the distance to TSS increases (Weber et al., 2010). The distribution of H2Av shows a similar pattern in heterochromatin but its signal decreases more sharply along the gene body compared to a moderate decline in euchromatic genes (Zhang

and Pugh 2011). Additionally, the highest H2Av signal is detected at promoters without well-defined core promoter elements such as a TATA box (Mavrich et al., 2008). Interestingly, genes with stalled RNA polymerase have less H2Av nucleosomes compared to those with elongated RNA polymerase (Weber et al., 2010). These results indicate that H2Av is able to enhance the nucleosome mobility probably through easy eviction, as H2Av nucleosome is relatively unstable.

Accelerating Biological Discoveries With Next-Generation Sequencing

The capability of obtaining DNA sequences with capillary electrophoresis-based Sanger sequencing developed in 1970s was a major break-through to modern Biology (Sanger et al., 1977). However, the main problem of Sanger sequencing is the need to separate samples using gels, which makes it difficult to apply to a large number of samples in parallel (Fei, 2014). Since 2005, the newly developed Next-Generation Sequencing (NGS) has made massively parallel sequencing possible. NGS is the catchall term used to describe a number of different modern sequencing technologies including: Illumina sequencing, Roche 454 sequencing, SOLiD sequencing, and so on. These sequencing technologies differ in various ways, but the major advances brought by NGS are the ability to produce tremendous amounts of data much more cheaply and rapidly. For example, the Illumina HiSeq® System is able to produce up to 3 billion reads in 1.5 to 11 days (Illumina, Inc).

There are three mainstream NGS technologies as mentioned above. Roche's 454 instruments use pyro-sequencing, which can produce read lengths up to 1 kb but requires complex sample preparation (Ronaghi et al., 1998). Applied Biosystem's SOLiD platform utilizes sequencing by ligation method (Kaczorowski et al., 1996). It has better accuracy than other sequencing methods but also requires relatively difficult sample preparation steps and it is reported to have issues sequencing palindromic sequences (Schuster, 2008). The most common NGS technology on the market is the Illumina sequencing platform, which is based on reversible dye-terminators technology (Bentley et al., 2008). It has relatively cheaper sample preparation steps; however, it can only produce up to 250 bp read lengths (Illumina, inc) compared with 1000 bp when using the Roche 454 (Roche Diagnostics GmbH, 2011).

Since the emergence of NGS, it has been widely used in various aspects of biological studies and has dramatically accelerated our understanding of unsolved issues from the Sanger sequencing era. Applying Chromatin Immunoprecipitation followed by NGS (ChIP-seq), researchers are able to identify regions bound by DNA binding proteins and the distribution of various modified histones. Specific DNA sites that physically interact with transcription factors and histones can be isolated and enriched by chromatin immunoprecipitation (ChIP), which produces a library of DNA fragments that bind to the protein of interest. These DNA fragments can be identified using NGS followed by whole-genome sequence databases analysis. ChIP-seq is capable of identifying binding patterns of DNA and proteins, such as conserved binding

motifs and distances to transcription starting site. RNA-sequencing (RNA-seq) is a technology that utilizes NGS to reveal the whole transcriptome profile at a given time (Chu et al., 2012). One of the typical applications of RNA-seq is to compare transcriptomes in different conditions, such as wild type vs. mutant animals and wild type vs. different treatments. RNA is purified from samples of interests and RNA libraries are produced by converting RNA into cDNA. NGS is then applied to sequence cDNA fragments, which are identified later using reference genome. RNA-seq provides the number of RNA reads counts representing transcription level of each gene. By adjusting RNA-seq protocols it also provides the ability to study a wide range of biological events, such as alternative gene splicing, SNPs and gene fusion (Maher, 2009). Additionally, using DNase I hypersensitive site sequencing (DNase-seq), the distribution of lightly packaged chromatin regions have been mapped, which provides information about DNA accessibility (Crawford et al., 2006).

References

Akhtar A and Becker PB. (2000). Activation of transcription through histone H4 acetylation by MOF, an acetyltransferase essential for dosage compensation in *Drosophila*. *Mol Cell*. 5(2):367-375.

Allfrey VG, Faulkner R and Mirsky AE. (1964). Acetylation and Methylation of Histones and Their Possible Role in the Regulation of Rna Synthesis. *Proc Natl Acad Sci U S A*, 51, 786-94

Arents G, Burlingame RW, Wang BC, Love WE, and Moudrianakis EN. (1991). The nucleosomal core histone octamer at 3.1 A˚ resolution: a tripartite protein assembly and a left-handed superhelix. *Proc. Natl. Acad. Sci. USA.* 88, 10148–10152.

Ausio J, and Abbott DW. (2002). The many tales of a tail: carboxyl-terminal tail heterogeneity specializes histone H2A variants for defined chromatin function. *Biochemistry*, 41, 5945–5949.

Baker SP and Grant PA. (2007). The SAGA continues: expanding the cellular role of a transcriptional co-activator complex. *Oncogene*. 26(37): 5329-40.

Bannister AJ and Kouzarides T. (2011). Regulation of chromatin by histone modifications. *Cell Res.* 21, 381–395

Barlow AL, van Drunen CM, Johnson CA, Tweedie S, Bird A, and Turner B M. (2001). dSIR2 and dHDAC6: Two Novel, Inhibitor-Resistant Deacetylases in Drosophila melanogaster. *Exp Cell Res*. 265(1), 90-103

Bentley DR, Balasubramanian S, Swerdlow HP, Smith GP, Milton J and Brown CG. (2008). Accurate whole human genome sequencing using reversible terminator chemistry. *Nature.* 456 (7218): 53-59.

Bernstein, BE, Humphrey EL, Erlich RL, Schneider R, Bouman P, Liu JS, Kouzarides T, Schreiber SL. (2002). Methylation of histone H3 Lys 4 in coding regions of active genes. *Proc. Natl Acad. Sci.* 99, 8695–8700

Bernstein BE, Mikkelsen TS, Xie X, Kamal M, Huebert DJ, Cuff J, Fry B, Meissner A, Werning M, Plath K, Jaenisch R, Wagschal A, Feil R, Scheriber SL and Lander ES. (2006). A bivalent chromatin structure marks key developmental genes in embryonic stem cells. *Cell.* 125, 315–326

Bonisch C and Hake SB. (2012). Histone H2A variants in nucleosomes and chromatin: more or less stable? *Nucleic Acids Res*. 40(21): 10719-41

Byvoet P. Shepherd GR, Hardin JM, and Noland BJ. (1972). The distribution and turnover of labeled methyl groups in histone fractions of cultured mammalian. *Arch Biochem Biophys*. 148(2):558-67.

Cai W, Wang C, Li Y, Yao C, Shen L, Liu S, Bao X, Schnable P, Girton J, Johansen J and Johansen KM. (2014). Genome-wide analysis of regulation of gene expression and H3K9me2 distribution by JIL-1 mediated histone H3S10 phosphorylation in *Drosophila*. *Nucleic Acids Res.* 42 : 5456-5467

Chadee DN, Hendzel MJ, Tylipski CP, Allis CD, Bazett-Jones DP and Wright JA. (1999). Increased Ser-10 phosphorylation of histone H3 in mitogen-stimulated and oncogene-transformed mouse fibroblasts. *J Biol Chem*. 274:24914-20

Chadwick BP and Willard HF. (2001). A novel chromatin pro- tein, distantly related to histone H2A, is largely excluded from the inactive X chromosome. *J. Cell Biol.* 152: 375–384

Cheung P, Allis CD and Sassone-Corsi P. (2000). Signaling to chromatin through histone modifications. *Cell.* 103:263-271.

Chu Y, Corey DR. (2012). RNA sequencing: platform selection, experimental design, and data interpretation. *Nucleic Acid Ther.* 22(4):271-4.

Cloos PA, Christensen J, Agger K, Maiolica A, Rappsilber J, Antal T, Hansen KH and Helin K. (2006). The putative oncogene GASC1 demethylates tri- and dimethylated lysine 9 on histone H3. *Nature* 442, 307–311.

Crawford GE, Holt IE, Whittle J, Webb BD, Tai D, Davis S, Margulies EH, Chen Y, Bernat JA, Ginsburg D, Zhou D, Luo S, Vasicek TJ, Daly MJ, Wolfsberg TG and Collins FS. (2006). Genome-wide mapping of DNase hypersensitive sites using massively parallel signature sequencing (MPSS). *Genome Res*. 16(1): 123-31.

Elgin SC and Reuter G. (2013). Position-effect variegation, hetero- chromatin formation, and gene silencing in Drosophila. *Cold Spring Harb Perspect Biol*. 5(8):a017780.

Feng, Q, Wang H, Ng HH, Erdjument-Bromage H, Tempst P, Struhl K and Zhang Y. (2002). Methylation of H3-lysine 79 is mediated by a new family of HMTases without a SET domain. *Curr. Biol*. 12, 1052–1058

Fernandez-Capetillo O, Lee A, Nussenzweig M and Nus-senzweig A. (2004). H2AX: The histone guardian of the genome. *DNA Repair (Amst.)* 3: 959–967.

Finch JT and Klug A. (1976) Solenoidal model for superstructure in chromatin. *Proc Natl Acad Sci*. 73(6):1897-1901.

Fischle W, Tseng BS, Dormann HL, Ueberheide BM, Garcia BA, Shabanowitz J, Hunt DF and Allis CD. (2005). Regulation of HP1-chromatin binding by histone H3 methylation and phosphorylation. *Nature*. 483: 1116-1122

Foglietti C, Filocamo G, Cundari E, De Rinaldis E, Lahm A, Cortese R and Steinkuhler C. (2006). Dissecting the biological functions of *Drosophila* histone deacetylases by RNA interference and transcriptional profiling. *J Biol Chem*, 281(26), 17968-76

Goto H, Yasui Y, Nigg EA and Inagaki M. (2002). Aurora-B phosphorylates Histone H3 at serine28 with regard to the mitotic chromosome condensation. *Genes Cells* 7, 11–-17

Gray SG and Ekström TJ. (2001). The Human Histone Deacetylase Family. *Exp Cell Res*, 262(2), 75-83

Grewal SI and Jia S. (2007). Heterochromatin revisited. *Nat Rev Genet* 8: 35-46.

Haempel K, Lange HW and Birkofer L. (1968). ε-N-trimethyllysine, a new amino acid in histones. *Naturwissenschaften* 55, 37

Hardy S, Jacques PE, Gevry N, Forest A, Fortin ME, Laflamme L, Gaudreau L, Robert F (2009) The euchromatic and heterochromatic landscapes are shaped by antagonizing effects of transcription on H2A.Z deposition. *PLoS Genet*. 5(10): e1000687

Hendzel MJ, Wei Y, Mancini MA, Van Hooser A, Ranalli T, Brinkley BR, Bazett-Jones DP and Allis CD. (1997) Mitosis-specific phosphorylation of histone H3 initiates primarily within pericentromeric heterochromatin during G2 and spreads in an ordered fashion coincident with mitotic chromosome condensation. *Chromosoma*. 106(6):348-360.

Henikoff S. (2008). Nucleosome destabilization in the epigenetic regulation of gene expression. *Nat Rev Genet.* 9:15-26.

Hines KA, Cryderman DE, Flannery KM, Yang H, Vitalini MW, Hazelrigg T, Mizzen CA and Wallrath L. (2009). Domains of HP1 Required for *Drosophila* melanogaster heterochromatin spreading. *Genetics*. 182: 967–77.

Hilfiker A, Hilfiker-Kleiner D, Pannuti A and Lucchesi JC. (1997) *mof*, a putative acetyl transferase gene related to the *Tip60* and *MOZ* human genes and to the *SAS* genes of yeast, is required for dosage compensation in *Drosophila*. *EMBO J.* 16:2054-2060.

Hodawadekar SC and Marmorstein R. (2007). Chemistry of acetyl trans- fer by histone modifying enzymes: structure, mechanism and implications for effector design. *Oncogene*. 26:5528- 5540.

Illumina, Inc. (2013). An Introduction to Next-Generation Sequencing Technology. Retrieved from http://res.illumina.com/documents/products/illumina_sequencing_introduction.pdf

Jenuwein T and Allis CD. (2001) Translating the histone code. *Science.* 10;293(5532):1074-80.

Kaczorowski T and Szybalski W. (1996). Co-operativity of hexamer ligation. *Gene*. 179 (1). 195–198

Kamakaka RT and Biggins S. (2005) Histone variants: deviants? *Genes Dev*. 1; 19(3):295-310.

Kornberg RD. (1974). Chromatin structure: a repeating unit of histones and DNA. *Science184*: 868-871.

Kouzarides T. (2007). Chromatin modifications and their function. *Cell.* 128:693-705.

Lachner M, O'Carroll D, Rea S, Mechtler K and Jenuwein T. (2001) Methylation of histone H3 lysine 9 creates a binding site for HP1 proteins. *Nature.* 410:116-120.

Lau AT, Lee SY, Xu YM, Zheng D, Cho YY and Zhu F. Phosphorylation of histone H2B serine 32 is linked to cell transformation. (2011). *J Biol Chem*. 286:26628- 37

Leach TJ, Mazzeo M, Chotkowski HL, Madigan JP, Wotring MG and Glaser RL. (2000). Histone H2A.Z is widely but nonrandomly distributed in chromosomes of *Drosophila melanogaster*. *J Biol Chem* 275(30):23267–23272.

Lee CK, Shibata Y, Rao B, Strahl BD and Lieb JD. (2004). Evidence for nucleosome depletion at active regulatory regions genome- wide. *Nat Genet*. 36:900-905.

Liaw H and Lustig AJ. (2006). Sir3 C-terminal domain involve- ment in the initiation and spreading of heterochromatin. *Mol Cell Biol.* 26: 7616–7631.

Luger K, Mader AW, Richmond RK, Sargent DF and Richmond TJ. (1997) Crystal structure of the nucleosome core particle at 2.8 Å resolution. *Nature.* 389:251-260.

Maher CA, Kumar-Sinha C, Cao X, Kalyana-Sundaram S ,Han B , Jing X, Sam L, Barrette T , Palanisamy N and Chinnaiya AM. (2009). Transcriptome sequencing to detect gene fusions in cancer. *Nature.* 458 (7234): 97-101

Malik HS and Henikoff S. (2003). Phylogenomics of the nucleosome. *Nat. Struct. Biol.* 10, 882–891.

Mateescu B, Bourachot B, Rachez C, Ogryzko V and Muchardt C. (2008). Regulation of an inducible promoterby an HP1b-HP1r switch. *EMBO*. 9: 267-72

Marzluff WF, Wagner EJ and Duronio RJ. (2008) Metabolism and regulation of canonical histone mRNAs: life without a poly(A) tail. *Nat. Rev. Genet*. 9, 843–854.

Mavrich TN, Jiang C, Ioshikhes IP, Li X, Venters BJ, Zanton SJ, Tomsho LP, Qi J, Glaser RL, Schuster SC, Gilmour DS, Albert I and Pugh BF. (2008). Nucleosome organization in the Drosophila genome. *Nature* 453(7193):358–362

Metzker ML. (2010) Sequencing technologies -the next generation. *Nat Rev Genet.* 2010 Jan;11(1):31-46.

Murray K. (1964). The occurrence of ε-N-methyl lysine in histones. *Biochemistry* 3, 10–15 (1964).

Nakayama J, Rice JC, Strahl BD, Allis CD and Grewal SI. (2001). Role of histone H3 lysine 9 methylation in epigenetic control of heterochromatin assembly. *Science* 292:110–113

Owen DJ, Ornaghi P, Yang JC, Lowe N, Evans PR, Ballario P, Neuhaus D, Filetici P and Travers AA. (2000). The structural basis for the recognition of acetylated histone H4 by the bromodomain of histone acetyltransferase gcn5p. *EMBO J.* 19 (22): 6141–9.

Paik WK and Kim S. (1967). ε-N-dimethyllysine in histones. *Biochem.Biophys. Res. Commun*. 27, 479–483.

Park YJ and Luger K. (2008). Histone chaperones in nucleosome eviction and histone exchange. *Curr Opin Struct Biol*. 18(3):282-9.

Pasini D, Malatesta M, Jung HR, Walfridsson J, Willer A, Olsson L, Skotte J, Wutz A, Porse B and Jensen ON. (2010). Characterization of an antagonistic switch between histone H3 lysine 27 methylation and acetylation in the transcriptional regulation of Polycomb group target genes. *Nucleic Acids Res.* 38:4958–4969

Poirier MG and Marko JF. (2002). Micromechanical studies of mitotic chromosomes. *J Muscle Res Cell Motil.* 23(5-6): 409-31.

Rando OJ. (2012). Combinatorial complexity in chromatin structure and function: revisiting the histone code. *Curr Opin Genet Dev*. 22:148–155.

Rea S, Eisenhaber F, O'Carroll D, Strahl BD, Sun ZW, Schmid M, Opravil S, Mechtler K, Ponting CP, Allis CD and Jenuwein T. (2000). Regulation of chromatin structure by site-specific histone H3 methyltransferases. *Nature*. 406(6796): 593-599.

Redon C, Pilch D, Rogakou E, Sedelnikova O, Newrock K and Bonner W. (2002). Histone H2A variants H2AX and H2AZ. *Curr. Opin. Genet. Dev*. 12: 162–169.

Richmond TJ, Rechsteiner T and Luger K. (1993). Studies of nucleosome structure. *Cold Spring Harb. Symp. Quant. Biol*. 58, 265–272.

Roche Diagnostics GmbH. (2011). GS FLX+ System: Sanger-like read lengths - the power of next-gen throughput, retrieved from http://454.com/downloads/GSFLXApplicationFlyer_FINALv2.pdf

Ronaghi M, Uhlen M and Nyren PA. (1998). A sequencing method based on real-time pyrophosphate. *Science*. 281(5375):363, 365.

Rossetto D, Avvakumov N and Cote J, (2012) Histone phosphorylation: a chromatin modification involved in diverse nuclear event. *Epigenetics* 7:10, 1098–1108

Sanger F, Nicklen S, and Coulson AR. (1977). DNA sequencing with chain-terminating inhibitors. *Proc Natl Acad Sci*. 74(12): 5463–5467.

Sassone-Corsi P, Mizzen CA, Cheung P, Crosio C, Monaco L, Jacquot S, Hanauer A and Allis CD. (1999) Requirement of Rsk-2 for epidermal growth factor-activated phosphorylation of histone H3. *Science.* 285:886-891.

Schuster SC. (2008). Next-generation sequencing transforms today's biology. *Nat. Methods.* 5(1): 16-8

Shi Y, Lan F, Matson C, Mulligan P, Whetstine JR, Cole PA, Casero RA and Shi Y. (2004). Histone demethylation mediated by the nuclear amine oxidase homologue LSD1. *Cell* 119, 941–953

Shogren-Knaak M, Ishii H, Sun JM, Pazin MJ, Davie JR and Peterson CL. (2006). Histone H4- K16 acetylation controls chromatin structure and protein interactions. *Science.* 311:844-847.

Smith MF, Athey BD, Williams SP and Langmore JP. (1990). Radial density distribution of chromatin: evidence that chromatin fibers have solid centers. *J. Cell Biol.* 110, 245–254

Song F, Chen P, Sun D, Wang M, Dong L, Liang D, Xu RM, Zhu P and Li G. (2014). Cryo-EM study of the chromatin fiber reveals a double helix twisted by tetranucleosomal units. *Science*. 344(6182):376-80

Strahl BD and Allis CD. (2000). The language of covalent histone modifications. *Nature.* 403, 41–45

Speiser C. (1974). Eine Hypothese uber die functionelle Organization der Chromosomen hoherer Organismen*. Theoret Appl Genet*. 44: 97–99.

Strelkov IS and Davie JR. (2002) Ser-10 phosphorylation of histone H3 and immediate early gene expression in oncogene-transformed mouse fibroblasts. *Cancer Res.* 62:75–78

Swaminathan J, Baxter EM and Corces VG. (2005) The role of histone H2Av variant replacement and histone H4 acetylation in the establishment of *Drosophila* heterochromatin. *Genes Dev.* 19:65–76.

Talbert PB, Ahmad K, Almouzni G, Ausio J, Berger F, Bhalla PL, Bonner WM, Cande WZ, Chadwick BP, Chan SW, Cross GA, Cui L, Dimitrov SI, Doenecke D, Eirin-Lopez JM, Gorovsky MA, Hake SB, Hamkalo BA, Holec S, Jacobsen SE, Kamieniarz K, Khochbin S, Ladurner AG, Landsman D, Latham JA, Loppin B, Malik HS, Marzluff WF, Pehrson JR, Postberg J, Schneider R, Singh MB, Smith MM, Thompson E, Torres-Padilla ME, Tremethick DJ, Turner BM, Waterborg JH, Wollmann H, Yelagandula R, Zhu B and Henikoff S. (2012) A unified phylogeny- based nomenclature for histone variants. *Epigenetics & Chromatin* 5:7.

Talbert PB and Henikoff S (2010). Histone variants—ancient wrap artists of the epigenome. *Nat Rev Mol Cell Biol* 11(4):264–275.

Talbert PB and Henikoff S. (2014). Environmental response mediated by histone variants. *Trends Cell Biol*. 24(11):642-50

Tan M, Luo H, Lee S, Jin F, Yang JS, Montellier E, Buchou T, Cheng Z, Rousseaux S, Rajagopal N, Lu Z, Ye Z, Zhu Q, Wysocka J, Ye Y, Khochbin S, Ren B and Zhao Y. (2011). Identification of 67 histone marks and histone lysine crotonylation as a new type of histone modification. *Cell* 146, 1016–1028.

Trojer P, Reinberg D. (2007). Facultative heterochromatin: Is there a molecular signature. *Mol Cell*. 28: 1–12.

Tse C, Sera T, Wolffe AP and Hansen JC (1998). Disruption of higher-order folding by core histone acetylation dramatically enhances transcription of nucleosomal arrays by RNA Polymerase III, *Mol. Cell. Biol*. 18 4629–4638.

Tsukada, Y. Fang J, Erdument-Bromage H, Warren ME, Borchers CH and Tempst P, Zhang Y. (2006). Histone demethylation by a family of JmjC domain-containing proteins. *Nature.* 439, 811–816.

Turner BM. (2005) Reading signals on the nucleosome with a new nomenclature for modified histones. *Nat Struct Mol Biol.* 12:110-112.

Wang, Y., W. Zhang, Y. Jin, J. Johansen and K.M. Johansen (2001) The JIL-1 tandem kinase mediates histone H3 phosphorylation and is required for maintenance of chromatin structure in *Drosophila*. *Cell.* 105 : 433-443.

Wang J, Lawry ST, Cohen AL and Jia S. (2014). Chromosome boundary elements and regulation of heterochromatin spreading Cell. *Mol. Life Sci*.71:4841–4852

Weber CM, Henikoff JG and Henikoff S. (2010). H2A.Z nucleosomes enriched over active genes are homotypic. *Nat. Struct. Mol. Biol*., 17, 1500–1507.

Wei Y, Yu L, Bowen J, Gorovsky MA and Allis CD. (1999) Phosphorylation of histone H3 is required for proper chromosome condensation and segregation. *Cell*. 97(1): 99-109.

Whetstine, JR, Nottke A, Lan F, Huarte M, Smolikov S, Chen Z, Spooner E, Li E, Zhang G, Colaiacovo M and Shi Y. (2006). Reversal of histone lysine trimethylation by the JMJD2 family of histone demethylases. *Cell* 125, 467–481.

Williams SP, Athey BD, Muglia LJ, Schappe RS, Gough AH and Langmore JP. (1986). Chromatin fibers are left-handed double helices with diameter and mass per unit length that depend on linker length. *Biophys J*, 49(1): 233-48

Wolffe AP. (1998). Chromatin: Structure and Function (San Diego, CA: Academic Press).

Wolffe AP and Hayes JJ. (1999). Chromatin disruption and modification. *Nucl Acids Res*. 27:711-720.

Woodcock CL, Horowitz RA. (1995). Chromatin organization re-viewed. *Trends Cell Biol*. 5(7): 272-7.

Woodcock CL, Frado LL and Rattner JB. (1984). The higher-order structure of chromatin: evidence for a helical ribbon arrangement. *J. Cell Biol*. 99, 42–52

Xhemalce B, Dawson MA and Bannister AJ. (2011). Histone modifications. In: Meyers R, ed. *Encyclopedia of Molecular Cell Bi- ology and Molecular Medicine*. John Wiley and Sons, 2011

Yang XJ and Seto E. (2008). Lysine Acetylation: Codified Crosstalk with Other Posttranslational Modifications. *Mol Cell*, 31(4), 449-461

Yao Fei. (2014) DNA Sequencing, Sanger and Next-Generation Sequencing, *Applications of Molecular genetics in Personalized Medicine.*(pp 3-10) Foster City, CA: OMICS Group eBooks.

Yaniv M. (2014). Chromatin remodeling: from transcription to cancer, *Cancer Genetics.* 207(9):352-357

Zentner GE and Henikoff S. (2013). Regulation of nucleosome dynamics by histone modifications. *Nat Struct Mol Biol.* 20:259–266

Zhang W, Jin Y, Ji Y, Girton J, Johansen J and Johansen KM. (2003). Genetic and phenotypic analysis of alleles of the Drosophila chromosomal JIL-1 kinase reveals a functional requirement at multiple developmental stages. *Genetics.* 165: 1341-54

Zhang, W., H. Deng, X. Bao, S. Lerach, J. Girton, J. Johansen and K.M. Johansen (2006) The JIL-1 histone H3S10 kinase regulates dimethyl histone H3K9 modifications and heterochromatic spreading in *Drosophila*. *Development.* 133 : 229-235.

Zhang Z and Pugh BF. (2011). Genomic organization of H2Av containing nucleosomes in Drosophila heterochromatin. *PLoS One.* 6(6): e20511.

Zhimulev IF and Belyaeva ES. (1975). Proposals to the problem of structural and functional organization of polytene chromosomes. *Theor. Appl. Genet*. 45, 335– 340.

Zhimulev IF. (1996). Morphology and structure of polytene chromosomes. *Adv Genet.* 34:1-497.

Zhimulev IF, Zykova TY, Goncharov FP, Khoroshko VA, Demakova OV, Semeshin VF, Pokholkova GV, Boldyreva LV, Demidova DS, Babenko VN, Demakov SA and Belyaeva ES. (2014), Genetic organization of interphase chromosome bands and interbands in Drosophila melanogaster. *PLos One*. Jul 29; 9(7):e101631

Zhou BO, Wang SS, Zhang Y, Fu XH, Dang W, Lenzmeier BA and Zhou JQ. (2011). Histone H4 Lysine 12 Acetylation Regulates Telomeric Heterochromatin Plasticity in Saccharomyces cerevisiae. *PLoS Genet*. 7(1):e1001272

Zippo A, Serafini R, Rocchigiani M, Pennacchini S, Krepelova A and Oliviero S. (2009). Histone crosstalk between H3S10ph and H4K16ac generates a histone code that mediates transcription elongation. *Cell*. 138(6): 1122-1136.

CHAPTER 3. DOMAIN REQUIREMENTS OF THE JIL-1 TANDEM KINASE FOR HISTONE H3S10 PHOSPHORYLATION AND CHROMATIN REMODELING IN VIVO

A paper published in the *The Journal of Biological Chemistry*

Yeran Li, Weili Cai, Chao Wang, Changfu Yao, Xiaomin Bao, Huai Deng, Jack Girton, Jørgen Johansen and Kristen M. Johansen

Summary

The JIL-1 kinase localizes to *Drosophila* polytene chromosome interbands and phosphorylates histone H3 at interphase counteracting histone H3 lysine9 (H3K9) dimethylation and gene silencing. JIL-1 can be divided into four main domains including an NH_2-terminal domain, two separate kinase domains, and a COOH-terminal domain. In this study we characterize the domain requirements of the JIL-1 kinase for H3S10 phosphorylation and chromatin remodeling in vivo. We show that a JIL-1 construct without the amino-terminal domain is without H3S10 phosphorylation activity despite that it localizes properly to polytene interband regions and that it contains both kinase domains. JIL-1 is a double kinase and we demonstrate that both kinase domains of JIL-1 are required to be catalytically active for H3S10 phosphorylation to occur. Furthermore, we provide evidence that JIL-1 is phosphorylated at serine424 and that this phosphorylation is necessary for JIL-1 H3S10 phosphorylation activity. Thus, these data are compatible with a model where the amino-terminal domain of JIL-1 is required for chromatin complex interactions that position the kinase domain(s) for catalytic activity in the context of the state of higher order nucleosome packaging and

chromatin structure, and where catalytic H3S10 phosphorylation activity mediated by the first kinase domain is dependent on autophosphorylation of serine424 by the second kinase domain. Furthermore, using a *lacO* repeat tethering system to target mutated JIL-1 constructs with or without catalytic activity we show that the epigenetic histone H3S10 phosphorylation mark itself functions as a causative regulator of chromatin structure independently of any structural contributions from the JIL-1 protein.

Introduction

In *Drosophila* histone H3S10 phosphorylation by the JIL-1 kinase at interphase functions to maintain active gene expression by serving as a protective epigenetic mark counteracting spreading of H3K9 dimethylation and gene silencing (1-5). Furthermore, JIL-1 is enriched about two-fold on the male X chromosome and implicated in dosage compensation of transcription due to its association with the male-specific lethal complex (6-9). JIL-1 is a Ser/Thr family tandem kinase that localizes specifically to euchromatic interband regions of polytene chromosomes (6,10). JIL-1 can be divided into four main domains including an amino-terminal domain (NTD), two kinase domains (KDI and KDII), and a carboxy-terminal domain (CTD) (6). It has previously been demonstrated that the CTD-domain of JIL-1 is sufficient for proper chromatin localization and for rescue of the grossly perturbed polytene chromosome morphology in *JIL-1* null mutants (3,11,12), and that a JIL-1 construct without the CTD-domain has kinase activity for histone H3S10 despite that it does not localize properly (3,12).

However, in these studies the properties of the NTD or the relative contributions of the two kinase domains were not determined. Thus, in order to further characterize the domain requirements of the JIL-1 kinase for H3S10 phosphorylation and regulation of chromatin structure, we generated a series of mutated JIL-1 constructs and expressed them in a *JIL-1* null mutant background. Our results showed that a JIL-1 construct without the NTD localizes properly to chromatin and rescues mutant polytene chromosome morphology. However, in immunocytochemistry and immunoblot analyses with H3S10ph antibody no histone H3S10 phosphorylation could be detected, strongly suggesting that the NTD domain is required for H3S10 kinase activity. Furthermore, we mutated either or both kinase domains to render them "kinase dead" and assessed their ability to phosphorylate H3S10. The results indicated that both kinase domains are required for kinase activity. In addition, using a LacI/*lacO*-repeat tethering system (13) we provide evidence that only JIL-1 constructs with H3S10 phosphorylation activity have the capacity to induce a change in higher order chromatin structure from a condensed heterochromatin-like band state to a more open euchromatic interband state.

Experimental Procedures

JIL-1 fusion constructs

The full-length LacI-JIL-1 construct (FL) was previously described by Deng et al. (13). LacI-tagged constructs from residue 1-926 lacking the COOH-terminal domain of JIL-1 (DCTD), a construct from residue 261-1207 lacking the NH_2-

terminal domain (DNTD), and a COOH-terminal domain construct from residue 927-1207 were cloned into the pUAST vector with the in frame DNA-binding domain of the lacI repressor from *E. coli* at the NH_2-terminus using standard methods (14). In addition, pUAST constructs were generated using the Transformer^{TM} Site-Directed Mutagenesis kit (ClonTech) to introduce K293A (KDI*) and K652A (KDII*) substitutions in the ATP-binding loops for each kinase domain as well as a double mutant combination (KDI*/KDII*). A QuikChange® Multi Site-Directed Mutagenesis Kit (Agilent) was used to introduce a S425A substitution into the first kinase domain of a full length JIL-1 cDNA. Subsequently, the mutated JIL-1 cDNA was cloned into the pUASP-HA-FLAG Gateway vector according to the manufacturer's instructions (Invitrogen). For protein purification a TAP-tagged JIL-1 construct from residue 261-1207 lacking the COOH-terminal domain (TAP-JIL-1) was cloned into the pUAST-NTAP vector (15). The TAP-tag consists of calmodulin binding peptide and Protein A. The fidelity of all constructs was verified by sequencing at the Iowa State University Sequencing facility.

Drosophila melanogaster stocks

Fly stocks were maintained at 25°C according to standard protocols (16). The *JIL-1^{z2}* null allele is described by Wang et al. (10) and Zhang et al. (17) whereas the Lac operator insertion line P11.3 and the GFP-lacI fusion line are described in Li et al. (18) and Danzer and Wallrath (19). All transgenic lines were generated by standard P-element transformation (BestGene, Inc.) and expression of the transgenes were driven using *Sgs3-GAL4* or *hsp70-GAL4* drivers introduced by

standard genetic crosses. Recombinant *JIL-1^{z2}, hsp70-GAL4* chromosomes were generated as described by Ji et al. (20). The *hsp70* promoter is leaky and was used without heat shock treatment as previously described (12). Expression levels of each of the JIL-1 constructs were monitored by immunoblot analysis as described below. All driver lines were obtained from the Bloomington Stock Center. Balancer chromosomes and markers are described by Lindsley and Zimm (21). Viability assays were performed by crossing *JIL-transgene/JIL-transgene ; JIL-1^{z2}/TM6* flies with *JIL-1^{z2} Hsp70-GAL4/TM6* flies. In these crosses the *TM6* chromosome was identified by the *Stubble* marker. Consequently, the experimental genotypes could be distinguished from balanced heterozygotic flies by absence of the *Stubble* marker. The expected Mendelian ratio of non-*Stubble* to *Stubble* flies assuming full rescue by the *JIL-1* transgenes in the *JIL-1* null background was 1:2 since *TM6/TM6* is embryonic lethal. Thus, the percentage of rescue of adult viability for each transgene was calculated as: observed non-*Stubble* flies X 200/observed *Stubble* flies. In each experiment the degree of rescue was determined on the basis of the analysis of the genotypes from at least 300 surviving progeny.

Immunohistochemistry

Standard polytene chromosome squash preparations were performed as described by Cai et al. (22) using either 1 or 5 min fixation protocols and labeled with antibody as described by Johansen et al. (23). Primary antibodies used for immunocytochemistry included rabbit anti-H3S10ph (Cell Signaling), Rabbit anti-H3K9me2 (Upstate Biotechnology), rabbit anti-JIL-1 (6), chicken anti-JIL-1 (7),

and anti-HA antibody (Roche). DNA was visualized by staining with Hoechst 33258 (Molecular Probes) in PBS. The appropriate species- and isotype-specific Texas Red-, TRITC-, and FITC-conjugated secondary antibodies (Cappel/ICN, Southern Biotech) were used (1:200 dilution) to visualize primary antibody labeling. The final preparations were mounted in 90% glycerol containing 0.5% *n*-propyl gallate. The preparations were examined using epifluorescence optics on a Zeiss Axioskop microscope and images were captured and digitized using a cooled Spot CCD camera. Images were imported into Photoshop where they were pseudocolored, image processed, and merged. In some images non-linear adjustments were made to the channel with Hoechst labeling for optimal visualization of chromosomes.

Immunoblot analysis

Protein extracts were prepared from adult flies or from dissected third instar larval salivary glands homogenized in a buffer containing: 20 mM Tris-HCl pH 8.0, 150 mM NaCl, 10 mM EDTA, 1 mM EGTA, 0.2% Triton X-100, 0.2% NP-40, 2 mM Na_3VO_4, 1 mM phenylmethylsulfonyl fluoride, 1.5 µg/ml aprotinin. Protein separation by SDS-PAGE and electroblot transfer were performed according to standard procedures (14). For these experiments we used the Bio-Rad Mini PROTEAN III system, electroblotting to 0.2 µm nitrocellulose with transfer buffer containing 20% methanol and in most cases including 0.04% SDS. Primary antibodies for immunoblot analysis included rabbit anti-H3S10ph (Cell Signaling), rabbit anti-histone H3 (Cell Signaling), rabbit anti-JIL-1 (6), chicken anti-JIL-1 (7) and mouse anti-lamin Dm0 (DSHB). The appropriate anti-mouse or anti-rabbit

HRP-conjugated secondary antibody (Bio-Rad) (1:3000) was used for visualization of primary antibody. Antibody labeling was visualized using chemiluminescent detection methods (SuperSignal West Pico Chemiluminescent Substrate, Pierce). The immunoblots were digitized using a flatbed scanner (Epson Expression 1680).

Protein purification and mass spectrometry

For TAP-JIL-1 fusion protein purification, the expressed protein was purified from protein extracts of 200 third instar larval salivary glands homogenized in a lysis buffer containing: 20 mM Tris-HCl pH 8.0, 150 mM NaCl, 10 mM EDTA, 1 mM EGTA, 0.2% Triton X-100, 0.2% Nonidet P-40, 2 mM Na_3VO_4, 1 mM dithiothreitol, 1 mM phenylmethylsulfonyl fluoride, and 1.5 µg/ml Aprotinin. Protein lysate was incubated with IgG agarose beads (Sigma) for 3 h at 4°C on a rotation wheel. Bound protein beads were washed with lysis buffer five times. Subsequently, the bound proteins were separated on a 4–12% Tris-Glycine gradient gel (Bio-Rad) and stained with Coomassie-blue R250. The TAP-JIL-1 gel band was identified based on size and Coomassie-staining intensity and cut out of the gel. The cut band was reduced, alkylated with iodoacetamide, and sent to the UC-Davis Proteomics Core Facility for analysis with tandem mass spectrometry using standard methods. Tandem mass spectra were extracted, and charge states were deconvoluted and deisotoped by Scaffold, version 3.5.1. All MS/MS samples were analyzed using Sequest version 3.3 (Thermo Fisher Scientific). Sequest was set up to search the Uniprot *Drosophila melanogaster* database (November 2011; 55391 entries) along with 101 common laboratory

contaminant proteins (www.gpm.org/crap/), assuming the digestion enzyme trypsin. Sequest was searched with a fragment ion mass tolerance of 1.00 kDa and a parent ion tolerance of 20 PPM. Oxidation of methionine, acetylation of lysine, tri-methylation of arginine, iodoacetamide derivative of cysteine and phosphorylation of serine, threonine and tyrosine were specified in Sequest as variable modifications. Scaffold version 3.5.1 (Proteome Software Inc.) was used to validate MS/MS based peptide and protein identifications. Peptide identifications were accepted if they could be established at greater than 80.0% probability as specified by the Peptide Prophet algorithm (24). Protein identifications were accepted if they could be established at greater than 80.0% probability and contained at least two identified peptides. Protein probabilities were assigned by the Protein Prophet algorithm (25). Proteins that contained similar peptides and could not be differentiated based on MS/MS analysis alone were grouped to satisfy the principles of parsimony. Using these parameters, a false discovery rate was calculated as 1.7% on the peptide level and 0% on the protein level.

Results

JIL-1 transgene expression

In order to further explore the relative contributions of the different JIL-1 domains to H3S10 phosphorylation and chromatin remodeling we expressed four LacI-tagged JIL-1 UAS P-element insertion constructs transgenically in wild-type and *JIL-1* null mutant animals. A full-length construct (FL), a construct without the COOH-terminal domain (DCTD), a construct without the NH_2-terminal domain

(DNTD), and a construct containing only the COOH-terminal domain (CTD) were made (Fig. 1A). A DNTD construct has not been previously characterized; however, the LacI-tagged FL, DCTD, and CTD constructs used in this study had properties identical to those reported for similar GFP- or CFP-tagged JIL-1 constructs (3,12) (Figs. 1 and 2). A transgenic line was selected for each construct that expressed at levels comparable to those of endogenous JIL-1 using a *hsp-70-GAL4* driver line as illustrated in Fig. 1B. FL rescued all aspects of the *JIL-1* null mutant phenotype including polytene chromosome morphology (Fig. 2B), viability, and like endogenous JIL-1, FL was upregulated on the male X chromosome (data not shown). The DCTD lacks the COOH-terminal sequences required for proper chromatin localization leading to mislocalization of the protein (13). However, it does retain its in vivo kinase activity (Fig. 1C) resulting in ectopic histone H3S10 phosphorylation (12). The DCTD rescues autosome polytene chromosome morphology (Fig. 2B) but only partially rescues that of the male X chromosome in *JIL-1* null mutants (12). In contrast, the CTD largely restores *JIL-1* null mutant chromosome morphology (Fig. 2B) including that of the male X chromosome (12). Furthermore, when the CTD is expressed in a wild-type background it has a dominant-negative effect and displaces endogenous JIL-1 (12).

The NTD is required for H3S10 phosphorylation in vivo

In order to determine the properties of a JIL-1 construct without the amino-terminal domain we expressed the DNTD in a *JIL-1* null mutant background. As illustrated in Fig. 2B the DNTD restored polytene chromosome morphology to or

near that of wild-type preparations (Fig. 2A) and localized correctly to interband regions. Interestingly, in contrast to the DCTD, the DNTD was not able to phosphorylate histone H3S10 as documented by immunoblotting of salivary gland protein extracts in Fig. 1C. Furthermore, the polytene squash preparations from larvae expressing the DNTD showed that the heterochromatic H3K9me2 mark spread to the chromosome arms (Fig. 2B). Spreading on the X chromosome was especially pronounced in both males and females as was also the case in the *JIL-1* null background (Fig. 2A) and as when the CTD that also is without H3S10 kinase activity (Fig. 1C) was expressed (Fig. 2B). These findings are consistent with the hypothesis that the epigenetic H3S10ph mark itself is necessary for counteracting the spreading of H3K9 dimethylation. Moreover, the results indicate that the NTD of JIL-1 is required for H3S10 phosphorylation to occur in vivo.

H3S10 phosphorylation is sufficient for chromatin remodeling

We have previously shown that ectopic targeting of full length JIL-1 using a LacI-tethering system induces robust histone H3S10 phosphorylation and a change in higher order chromatin structure from a condensed heterochromatin-like state to a more open euchromatic state (13). However, the surprising finding that the CTD of JIL-1 alone is sufficient to rescue *JIL-1* null mutant chromosome defects including those of the male X chromosome restoring euchromatic interband regions (12) (Fig. 2B) raised the question whether the CTD also would be sufficient to cause ectopic chromatin remodeling independently of H3S10 phosphorylation. Therefore, we further explored the LacI-tethering paradigm by

targeting the various LacI-JIL-1 deletion constructs with and without kinase activity, including the CTD, to chromatin in a condensed heterochromatin-like state. As illustrated in Fig. 3 tethering of the FL or the DCTD construct to *lacO* repeats inserted into the middle of a polytene chromosome band in region 96C1-2 resulted in ectopic H3S10 phosphorylation and "opening" of the band. In contrast, targeting of GFP-LacI or the CTD resulted in neither H3S10 phosphorylation nor chromatin structure changes. In addition, as illustrated in Fig. 3 the CTD displaces endogenous JIL-1 as previously reported (12), leading to a striking decrease in the levels of histone H3S10 phosphorylation in the interband polytene chromosome regions. Thus, these findings strongly indicate that the CTD of JIL-1 does not contribute to "opening" of the band when full length JIL-1 is targeted but rather that these chromatin structure changes are caused solely by H3S10 phosphorylation. Supporting this conclusion, when the DNTD was targeted it accumulated at the target site without any detectable H3S10 phosphorylation or chromatin decondensation and similarly to the CTD resulted in decreased overall levels of H3S10 phosphorylation. However, expression of the DNTD additionally induced chromatin structure perturbations, especially at the targeting site, as well as ectopic contacts between non-homologous chromatin regions. These results suggest that expression of the DNTD, like expression of the CTD, reduced global H3S10 phosphorylation levels by displacing native JIL-1 from the normal binding sites of JIL-1 but that the DNTD had an additional dominant-negative effect due to the presence of the two kinase domains.

JIL-1 mediated H3S10 phosphorylation requires that both kinase domains are catalytically active

It has recently been demonstrated that a "kinase dead" version of full-length JIL-1 (KDI*/KDII*) in which the crucial lysine for catalytic activity in each of the two kinase domains (K^{293} and K^{652}) was changed to alanine is without kinase activity (13) in a *JIL-1* null mutant background. However, these experiments did not address whether one or both kinase domains are functional and required for H3S10 phosphorylation activity. Therefore, we made two additional constructs (KDI* and KDII*) in each of which only one of the lysines was changed to an alanine as diagrammed in Fig. 4A and expressed them in a *JIL-1* mutant background. A transgenic line was selected for each construct that expressed at levels comparable to those of endogenous JIL-1 using a *hsp70-GAL4* driver (Fig. 4B). The results showed that the properties of both the single kinase "dead" versions, KDI* and KDII*, were indistinguishable from those obtained by expressing a construct where both kinase domains (KDI*/KDII*) were mutated. As illustrated in Fig. 4C none of the three constructs were able to phosphorylate histone H3S10 as documented by immunoblotting of salivary gland protein extracts. Furthermore, in polytene squash preparations from *JIL-1* null larvae expressing KDI*, KDII*, or KDI*/KDII* (Fig. 5) there was no rescue of chromosome morphology and spreading of the H3K9me2 mark to the chromosome arms was similar to that observed in *JIL-1* null preparations (Fig. 2A). These results strongly indicate that both kinase domains of JIL-1 are required to be catalytically active for H3S10 phosphorylation to occur.

Phosphorylation of Ser424 is required for JIL-1 H3S10 kinase activity

Phylogenetic analysis suggests that JIL-1 is most closely related to the mammalian tandem mitogen and stress-activated kinases 1 and 2 (MSK1/2) in a clade with 95% bootstrap support that is distinct from the RSK (ribosomal S6 p90 kinase) family of tandem kinases (26). The amino-terminal kinase domain of JIL-1 shares 63% amino acid identity with the corresponding domain in human MSK1 but only 47% identity with that of *Drosophila* RSK (6). MSKs regulate transcription by phosphorylation of transcription factors, including CREB and ATF1 (27), and chromatin associated proteins, including HMG-14 and histone H3 (28,29). Similarly to JIL-1 MSK1/2 phosphorylates H3 at Ser10 (29); however, unlike JIL-1 (30,31) MSK1/2 additionally has H3S28 phosphorylation activity (29,32). The molecular mechanisms of MSK activation is complex and requires multisite phosphorylation by upstream kinases and subsequent autophophorylation of Ser212 and Ser376 by its carboxy-terminal kinase domain (33,34). The JIL-1 kinase is constitutively active and is autophosphorylated (6,30). Moreover, the region in human MSK1 containing Ser212 in the amino-terminal kinase domain is highly conserved in JIL-1 ($MSK1^{S212}$ corresponds to $JIL\text{-}1^{424}$, Fig. 6A) whereas the residue corresponding to $MSK1^{S376}$ in the linker region has been substituted with a threonine in JIL-1 ($JIL\text{-}1^{T589}$). Thus, to investigate whether these residues also play a role in JIL-1 activity in vivo we expressed a tandem-affinity tagged JIL-1 construct that included the amino-terminal domain, the two kinase domains, and the linker region (TAP-JIL-1) transgenically in flies. The expressed protein was purified from protein extracts

of third instar larval salivary glands, separated using SDS-PAGE, and the enriched TAP-JIL-1 band identified by size and Coomassie Blue staining was cut out and analyzed by tandem mass spectrometry for phosphorylated residues. Of the five peptides recovered containing JIL-1^{T589} none were phosphorylated; however, in six peptides out of ten containing JIL-1^{S424} this residue was phosphorylated. Thus, these results indicate that in salivary glands JIL-1 is phosphorylated at Ser424 but not at detectable levels at Thr589. No other phosphorylated sites were identified in the samples.

In order to determine whether phosphorylation of Ser424 is required for H3S10 kinase activity we made a JIL-1 construct where Ser424 was mutated to an alanine (JIL-1^{S424A}, Fig. 6B) and expressed it transgenically in a *JIL-1* mutant background. A transgenic line was selected that expressed at levels comparable to those of endogenous JIL-1 using a *hsp70-GAL4* driver (Fig. 6D). As illustrated in Fig. 6D JIL-1^{S424A} had little or no histone H3S10 phosphorylation activity as documented by immunoblotting of salivary gland protein extracts. Furthermore, in polytene squash preparations from *JIL-1* null larvae expressing JIL-1^{S424A} (Fig. 6C) there was no detectable H3S10 phosphorylation and spreading of the H3K9me2 mark to the chromosome arms was similar to that observed in *JIL-1* null preparations (Fig. 2A). These results strongly indicate that phosphorylation of Ser424 is required for JIL-1 to be catalytically active and for H3S10 phosphorylation to occur. However, it should be noted that although chromosome morphology was still perturbed in *JIL-1* null preparations expressing

the JIL-1^{S424A} construct the morphology was discernibly improved compared to preparations expressing KDI*, KDII*, or KDI*/KDII* (Fig. 5).

The properties of the JIL-1 constructs analyzed in the present study including viability are summarized in Table 1. The homozygous *JIL-1*^{z2} genotype is a late larval lethal with no escapers (17). Interestingly, all of the deletion and mutated constructs with or without H3S10 phosphorylation activity restored some degree of viability indicating as previously suggested (12) that multiple and independent mechanisms may be contributing to the lethality of the *JIL-1* null mutant.

Discussion

In this study we show that a JIL-1 construct without the amino-terminal domain is without H3S10 phosphorylation activity despite that it localizes properly to polytene interband regions and that it contains both kinase domains. This is in contrast to a JIL-1 construct without the carboxy-terminal domain, that although mislocalized to ectopic chromatin regions retains its H3S10 phosphorylation capability (12; this study). Interestingly, although the CTD of JIL-1 binds to the amino-terminal tail of histone H3 modeling of the 3D-structure of JIL-1 relative to nucleosome structure suggested that JIL-1 is likely to phosphorylate H3 of one or more nucleosomes some distance away from this binding site (W. Cai, unpublished results). Taken together these findings suggest a model where the NTD of JIL-1 is required for chromatin complex interactions that position the kinase domain(s) for catalytic activity in the context of the state of higher order nucleosome packaging and chromatin structure whereas sequences in the CTD

mediate binding to specific chromatin sites. Furthermore, it has been demonstrated that sequences within both the NTD and CTD are required for enrichment of JIL-1 on the male X chromosome (12).

JIL-1 is a double kinase raising the question of the function and relative contributions of the two kinase domains. In this study we show that the properties of both the single kinase "dead" versions of JIL-1, KDI* and KDII*, were indistinguishable from those obtained by expressing a construct where both kinase domains (KDI*/KDII*) were mutated. Neither construct was able to phosphorylate H3S10, rescue *JIL-1* null polytene chromosome morphology, or prevent spreading of the H3K9me2 silencing mark, strongly indicating that both kinase domains of JIL-1 are required to be catalytically active for H3S10 phosphorylation to occur. Furthermore, we provide evidence that JIL-1 is phosphorylated at Ser424 in vivo and that this phosphorylation is required for JIL-1 H3S10 phosphorylation activity. This phosphorylation site is conserved in the mammalian MSK family of tandem kinases that are the closest homologs in the databases to the JIL-1 kinase (26). Upon activation of MSKs by upstream kinases, this site has been demonstrated to be autophosphorylated by the carboxy-terminal MSK kinase domain and to be required for catalytic activity (33,34). Thus, the data presented here are compatible with a model where autophosphorylation of Ser424 by the second kinase domain of JIL-1 is similarly required for catalytic activity and H3S10 phosphorylation mediated by the first kinase domain. The molecular mechanism of MSK activation involves multisite phosphorylation that is context and pathway dependent (33,34). In contrast, the

JIL-1 kinase is constitutively active (6,30) and therefore the requirements for its activation are likely to be less complex. Supporting this hypothesis we did not find evidence for phosphorylation of other sites than Ser424 including Thr589, the corresponding residue of which autophosphorylation is required for activation of the MSKs.

An important issue of epigenetic chromatin structure regulation by histone phosphorylation is whether the H3S10ph mark itself has the capacity to induce chromatin changes or whether it only plays a reinforcing or maintenance role. Using a LacI tethering system Deng et al. (13) provided evidence that ectopic histone H3S10 phosphorylation by the JIL-1 kinase is sufficient to cause striking changes in chromatin packaging from a condensed to an open state. This effect was absent when a "kinase dead" LacI-JIL-1 construct that is without histone H3S10 phosphorylation activity was expressed (13). This indicates that the observed chromatin structure changes depended on JIL-1 kinase-mediated histone H3S10 phosphorylation and not on the tethering of the LacI-JIL-1 construct itself. However, the surprising finding that the CTD of JIL-1 alone is sufficient to rescue *JIL-1* null mutant chromosome defects including those of the male X chromosome, restoring euchromatic interband regions, suggested that alternative or redundant mechanisms of direct chromatin structure modification may be mediated by the CTD (12). One possibility is that the CTD may serve as a binding platform for an unidentified protein or protein complex that has the ability to induce changes in chromosome morphology but which can function only after proper localization through interactions with the CTD of JIL-1. Another

possibility is that binding of the CTD to chromatin by itself is sufficient to alter chromatin structure through bridging interactions with surrounding molecules. However, in this study we demonstrate using the same experimental paradigm as Deng et al. (13) that LacI mediated tethering of neither the CTD nor the DNTD of JIL-1 resulted in H3S10 phosphorylation or transformation of a polytene chromatin band into an interband, and that such chromatin remodeling only is effectuated by JIL-1 constructs with H3S10 kinase activity. Thus, these findings provide further evidence that the epigenetic histone H3S10 phosphorylation mark itself functions as a causative regulator of chromatin structure independently of any structural contributions from the JIL-1 protein.

References

1. Zhang, W., Deng, H., Bao, X., Lerach, S., Girton, J., Johansen, J., and Johansen, K.M. (2006) The JIL-1 histone H3S10 kinase regulates dimethyl H3K9 modifications and heterochromatic spreading in *Drosophila*. *Development* **133,** 229-235.

2. Deng, H., Cai, W., Wang C., Lerach, S., Delattre M., Girton, J., Johansen, J., and Johansen, K.M. (2010) *JIL-1* and *Su(var)3-7* interact genetically and counterbalance each others' effect on position effect variegation in *Drosophila*. *Genetics* **185**, 1183-1192.

3. Wang, C., Cai, W., Li, Y., Deng, H., Bao, X., Girton, J., Johansen, J., and Johansen, K.M. (2011) The epigenetic H3S10 phosphorylation mark is required for counteracting heterochromatic spreading and gene silencing in *Drosophila melanogaster*. *J. Cell Sci.* **124,** 4309-4317.

4. Wang, C., Girton, J., Johansen, J., and Johansen, K.M. (2011) A balance between euchromatic (JIL-1) and heterochromatic (SU(VAR)2-5 and SU(VAR)3-9) factors regulates position-effect variegation in Drosophila. *Genetics* **188,** 745-748.

5. Wang, C., Cai, W., Li, Y., Girton, J., Johansen, J., and Johansen, K.M. (2012) H3S10 phosphorylation by the JIL-1 kinase regulates H3K9

dimethylation and gene expression at the *white* locus in *Drosophila. Fly* **6,** 1-5.

6. Jin, Y., Wang, Y., Walker, D.L., Dong, H., Conley, C., Johansen, J., and Johansen, K.M. (1999) JIL-1: a novel chromosomal tandem kinase implicated in transcriptional regulation in *Drosophila*. *Mol. Cell* **4,** 129-135.

7. Jin, Y., Wang, Y., Johansen, J., and Johansen, K.M. (2000) JIL-1, a chromosomal kinase implicated in regulation of chromatin structure, associates with the MSL dosage compensation complex. *J. Cell Biol.* **149,** 1005-1010.

8. Lerach, S., Zhang, W., Deng, H., Bao, X., Girton, J., Johansen, J., and Johansen, K.M. (2005) JIL-1 kinase, a member of the male-specific lethal (MSL) complex, is necessary for proper dosage compensation of eye pigmentation in *Drosophila*. *Genesis* **43,** 213-215.

9. Wang, C.I., Alekseyenko, A.A., LeRoy, G., Elia, A.E.H., Gorchakov, A.A., Britton, L.-M.P., Elledge, S.J., Kharchenko, P.V., Garcia, B.A., and Kuroda, M.I. (2013) Chromatin proteins captured by ChIP-mass spectrometry are linked to dosage compensation in *Drosophila*. *Nat. Struc. Mol. Biol.* **20,** 202-209.

10. Wang, Y., Zhang, W., Jin, Y., Johansen, J., and Johansen, K.M. (2001) The JIL-1 tandem kinase mediates histone H3 phosphorylation and is required for maintenance of chromatin structure in *Drosophila*. *Cell* **105,** 433-443.

11. Deng, H., Zhang, W., Bao, X., Martin, J.N., Girton, J., Johansen, J., and Johansen, K.M. (2005) The JIL-1 kinase regulates the structure of *Drosophila* polytene chromosomes. *Chromosoma* **114,** 173-182.

12. Bao, X., Cai, W., Deng, H., Zhang, W., Krencik, R., Girton, J. and Johansen, K.M. (2008) The COOH-terminal domain of the JIL-1 histone H3S10 kinase interacts with histone H3 and is required for correct targeting to chromatin. *J. Biol. Chem.* **283**, 32741-32750.

13. Deng, H., Bao, X., Cai, W., Blacketer, M.J., Belmont, A.S., Girton, J., Johansen, J., and Johansen, K.M. (2008) Ectopic histone H3S10 phosphorylation causes chromatin structure remodeling in *Drosophila. Development* **135,** 699-705.

14. Sambrook, J. and Russell, D. W. (2001) *Molecular Cloning: A Laboratory Manual*. Cold Spring Harbor Laboratory, Cold Spring Harbor, NY.

15. Veraksa, A., Baur, A., and Artavanis-Tsakonas, S. (2005) Analyzing protein complexes in *Drosophila* with tandem affinity purification mass spectrometry. *Dev. Dyn.* **232,** 827-834.

16. Roberts, D.B. (1998) *Drosophila: A Practical Approach.* 2nd ed, IRL Press, Oxford, UK.

17. Zhang, W., Jin, Y., Ji, Y., Girton, J., Johansen, J., and Johansen, K.M. (2003) Genetic and phenotypic analysis of alleles of the *Drosophila* chromosomal JIL-1 kinase reveals a functional requirement at multiple developmental stages. *Genetics* **165,** 1341-1354.

18. Li, Y., Danzer, J.R., Alvarez, P., Belmont, A.S., and Wallrath, L.L. (2003) Effects of tethering HP1 to euchromatic regions of the *Drosophila* genome. *Development* **130,** 1817-1824.

19. Danzer, J.R., and Wallrath, L.L. (2004) Mechanisms of HP1-mediated gene silencing in *Drosophila*. *Development* **131,** 3571-3580.

20. Ji, Y., Rath, U., Girton, J., Johansen, K.M., and Johansen, J. (2005) D-Hillarin, a novel W180-domain protein, affects cytokinesis through interaction with the septin family member Pnut. *J. Neurobiol.* **64,** 157-169.

21. Lindsley, D.L., and Zimm, G.G. (1992) *The genome of Drosophila melanogaster*. Academic Press, New York, NY.

22. Cai, W., Jin, Y., Girton, J., Johansen, J., and Johansen, K.M. (2010) Preparation of polytene chromosome squashes for antibody labeling. *J. Vis. Exp.* http://www.jove.com/index/Details.stp?ID=1748. doi: 10.3791/1748.

23. Johansen, K.M., Cai, W., Deng, H., Bao, X., Zhang, W., Girton, J., and Johansen, J. (2009) Methods for studying transcription and epigenetic chromatin modification in *Drosophila* polytene chromosome squash preparations using antibodies. *Methods* **48,** 387-397.

24. Keller, A., Nesvizhskii, A.I., Kolker, E., and Aebersold, R. (2002) Empirical statistical model to estimate accuracy of peptide identifications made by MS/MS and database search. *Anal. Chem.* **74,** 5383-5392.

25. Nesvizhskii, A.I., Keller, A., Kolker, E., and Aebersold, R. (2003) A statistical model for identifying proteins by tandem mass spectrometry. *Anal. Chem.* **75,** 4646-4658.

26. Johansen, K.M., Johansen, J., Jin, Y., Walker, D.L., Wang, D., and Wang, Y. (1999) Chromatin structure and nuclear remodeling. *Crit. Rev. Eukaryotic Gene Expr.* **9,** 267-277.

27. Wiggin, G.R., Soloaga, A., Foster, J.M., Murray-Tait, V., Cohen, P., and Arthur, J.S. (2002) MSK1 and MSK2 are required for the mitogen- and stress-induced phosphorylation of CREB and ATF1 in fibroblasts. *Mol. Cell. Biol.* **22,** 44-48.

28. Thomson, S., Clayton, A.L., Hazzalin, C.A., Rose, S., Barratt, M., and Mahadevan, L.C. (1999) The nucleosomal response associated with immediate-early gene induction is mediated via alternative MAP kinase cascades: MSK1 as a potential H3/HMG-14 kinase. *EMBO J.* **18,** 4779-4793.

29. Soloaga, A., Thomson, S., Wiggin, G.R., Rampersaud, N., Dyson, M.H., Hazzalin, C.A., Mahadevan, L.C., and Arthur, J.S. (2003) MSK2 and MSK1 mediate the mitogen- and stress-induced phosphorylation of histone H3 and HMG-14. *EMBO J.* **22,** 2788-2797.

30. Regnard, C., Straub, T., Mitterweger, A., Dahlsveen, I.K., Fabian, V., and Becker, P.B. (2011) Global analysis of the relationship between JIL-1 kinase and transcription. *PLoS Genetics* **7,** e1001327. doi: 10.1371/journal.pgen.1001327.

31. Wang, C., Yao, C., Li, Y., Cai, W., Bao, X., Girton, J., Johansen, J., and Johansen, K.M. (2013) Evidence against a role for the JIL-1 kinase in H3S28 phosphorylation and 14-3-3 recruitment to active genes in *Drosophila*. *PLoS ONE* **8,** e62484. doi: 10.1371/journal.pone.0062484.

32. Dyson, M.H., Thomson, S., Inagaki, M., Goto, H., Arthur, S.J., Nightingale, K., Iborra, F.J., and Mahadevan, L.C. (2005) MAP kinase-mediated phosphorylation of distinct pools of histone H3 at S10 or S28 via mitogen- and stress-activated kinase 1/2. *J. Cell Sci.* **118,** 2247-2259.

33. McCoy, C.E., Campbell, D.G., Deak, M., Bloomberg, G.B., and Arthur, J.S.C. (2005) MSK1 activity is controlled by multiple phosphorylation sites. *Biochem. J.* **387,** 507-517.

34. McCoy, C.E., MacDonald, A., Morrice, N.A., Campbell, D.G., Deak, M., Toth, R., McIlrath, J., and Arthur, J.S.C. (2007) Identification of novel phosphorylation sites in MSK1 by precursor ion scanning MS. *Biochem. J.* **402,** 491-501.

Figures

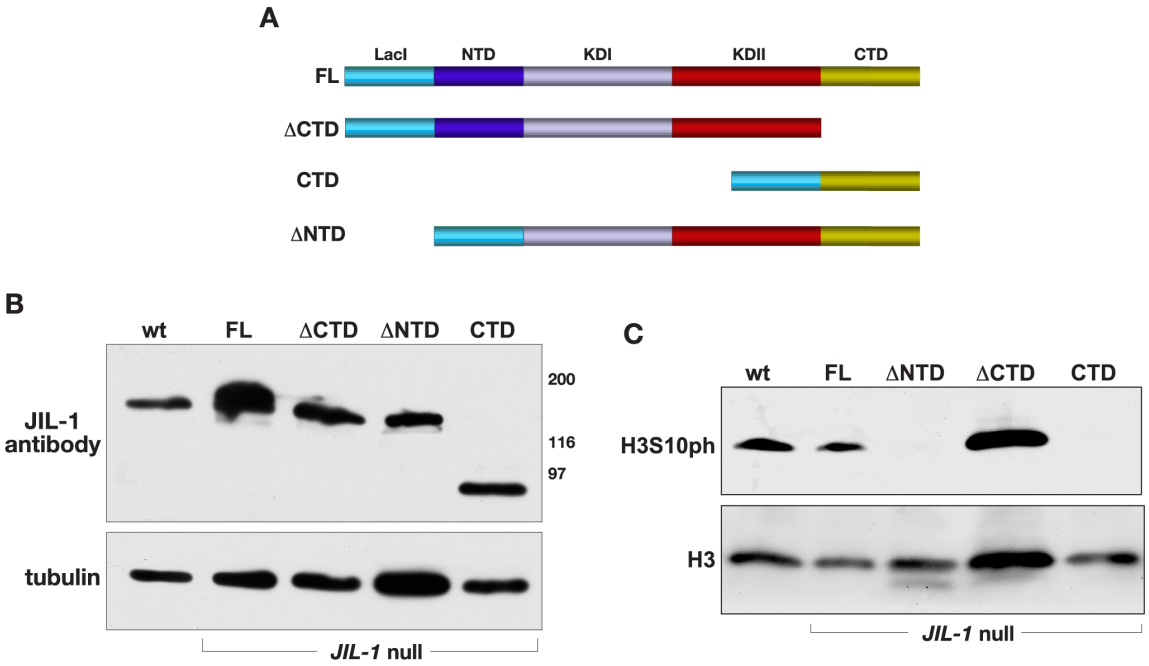

FIGURE 1. **Expression of transgenic JIL-1 constructs in a *JIL-1* null background.** (A) Diagrams of the JIL-1 LacI-tagged constructs analyzed. (B) Immunoblot labeled with JIL-1 antibody of protein extracts from wild type (wt) and from *JIL-1* null salivary glands expressing the FL, the DCTD, the DNTD, and the CTD, respectively. Labeling with tubulin antibody was used as a loading control. The relative migration of molecular size markers is indicated to the right of the immunoblot in kDa. (C) Immunoblot labeled with H3S10ph antibody of protein extracts from salivary glands from wild type third instar larvae (wt), and from *JIL-1* null salivary glands expressing the FL, the DCTD, the DNTD, and the CTD, respectively. Labeling with histone H3 antibody was used as a loading control.

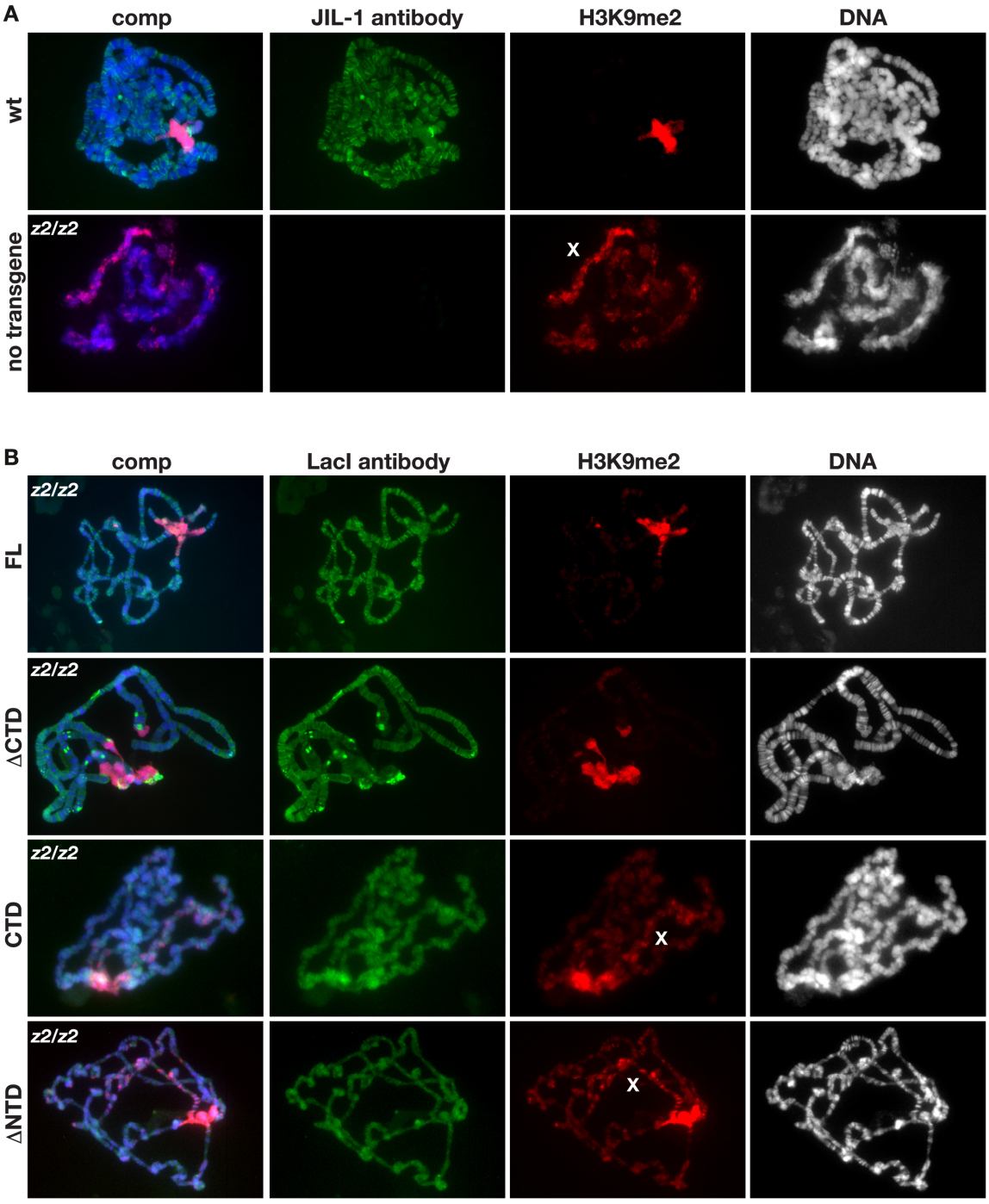

FIGURE 2. **Immunocytochemical analysis of polytene chromosome morphology and histone H3K9 dimethylation in *JIL-1* null larvae expressing *JIL-1* transgenes.** (A) Comparison of polytene chromosome squash preparations from wild-type (wt) and *JIL-1* null (*z2/z2*) third instar larval salivary glands labeled with JIL-1 antibody. (B) Polytene chromosome squash preparations from *JIL-1* null (*z2/z2*) third instar larval salivary glands expressing

the FL, the DCTD, the DNTD, and the CTD, respectively. Transgenic protein localization (in green) was identified using LacI antibody, histone H3K9 dimethylation (in red) was identified using H3K9me2 antibody, and DNA (in blue or gray) was labeled by Hoechst.

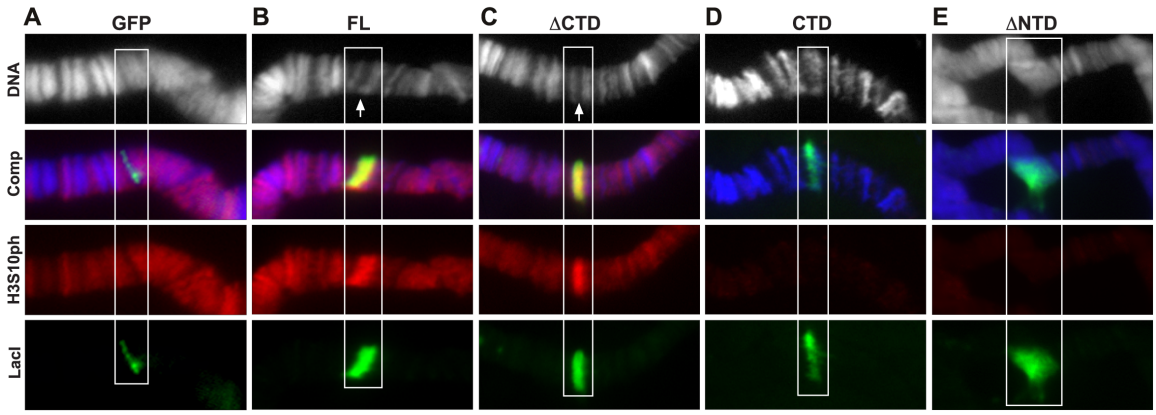

FIGURE 3. **Tethering of LacI-tagged JIL-1 constructs to a polytene chromosome band *LacO* insertion site.** The panels show triple labelings of polytene squash preparations from third instar larvae homozygous for the *lacO* repeat line P11.3 which is inserted into the middle of a polytene band in region 96C1-2. GFP was tethered to the *lacO* repeats in (A), FL in (B), DCTD in (C), CTD in (D), and DNTD in (E). LacI antibody labeling is shown in green, H3S10ph antibody labeling in red, and Hoechst labeling of DNA in blue or grey. The white boxes indicate the location of the polytene band with the *lacO* repeat insertion site. The white arrows indicate the "split" in the polytene bands reflecting decondensation of the chromatin when FL or DCTD is tethered to the band in contrast to its wild-type morphology when GFP, CTD, or DNTD is tethered and where there is no ectopic upregulation of histone H3S10 phosphorylation. Note: expression of the CTD and DNTD has a dominant negative effect and displaces endogenous JIL-1 resulting in a chromosome-wide reduction in the levels of H3S10ph at interband regions (D and E).

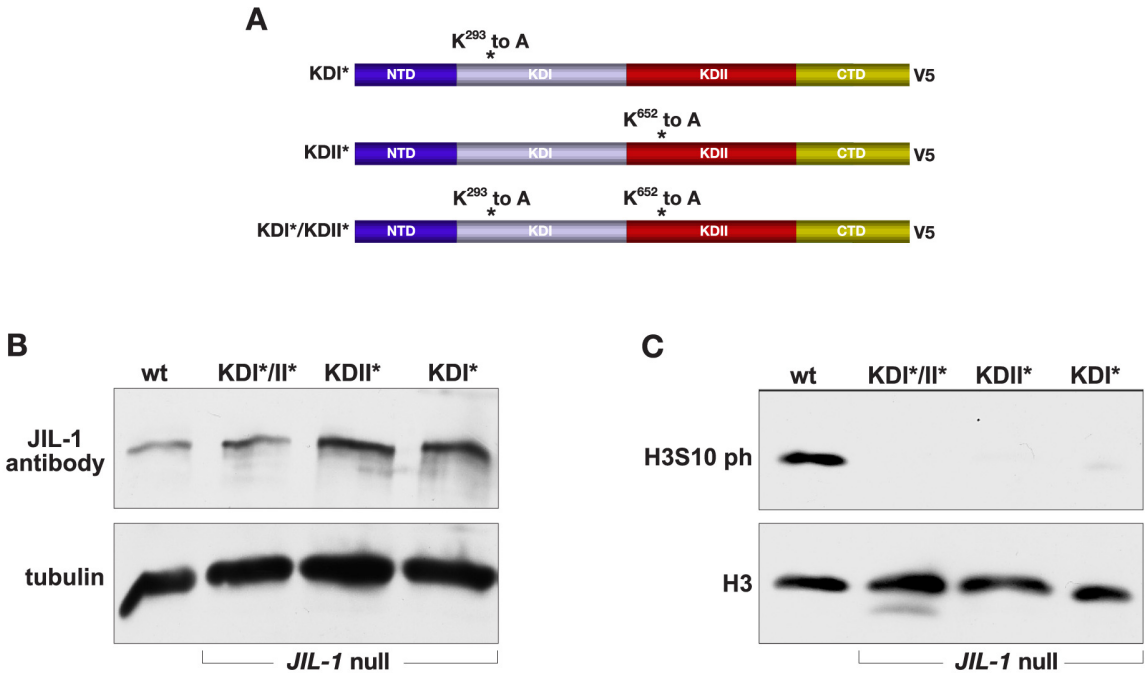

FIGURE 4. **Expression of transgenic JIL-1 "kinase dead" constructs in a *JIL-1* null background.** (A) Diagrams of the JIL-1 V5-tagged constructs analyzed. (B) Immunoblot labeled with JIL-1 antibody of protein extracts from wild type (wt) and from *JIL-1* null salivary glands expressing the KDI*/KDII*, KDII*, and KDI*, respectively. Labeling with tubulin antibody was used as a loading control. (C) Immunoblot labeled with H3S10ph antibody of protein extracts from salivary glands from wild type third instar larvae (wt), and from *JIL-1* null salivary glands expressing the KDI*/KDII*, and KDII*, and KDI*, respectively. Labeling with histone H3 antibody was used as a loading control.

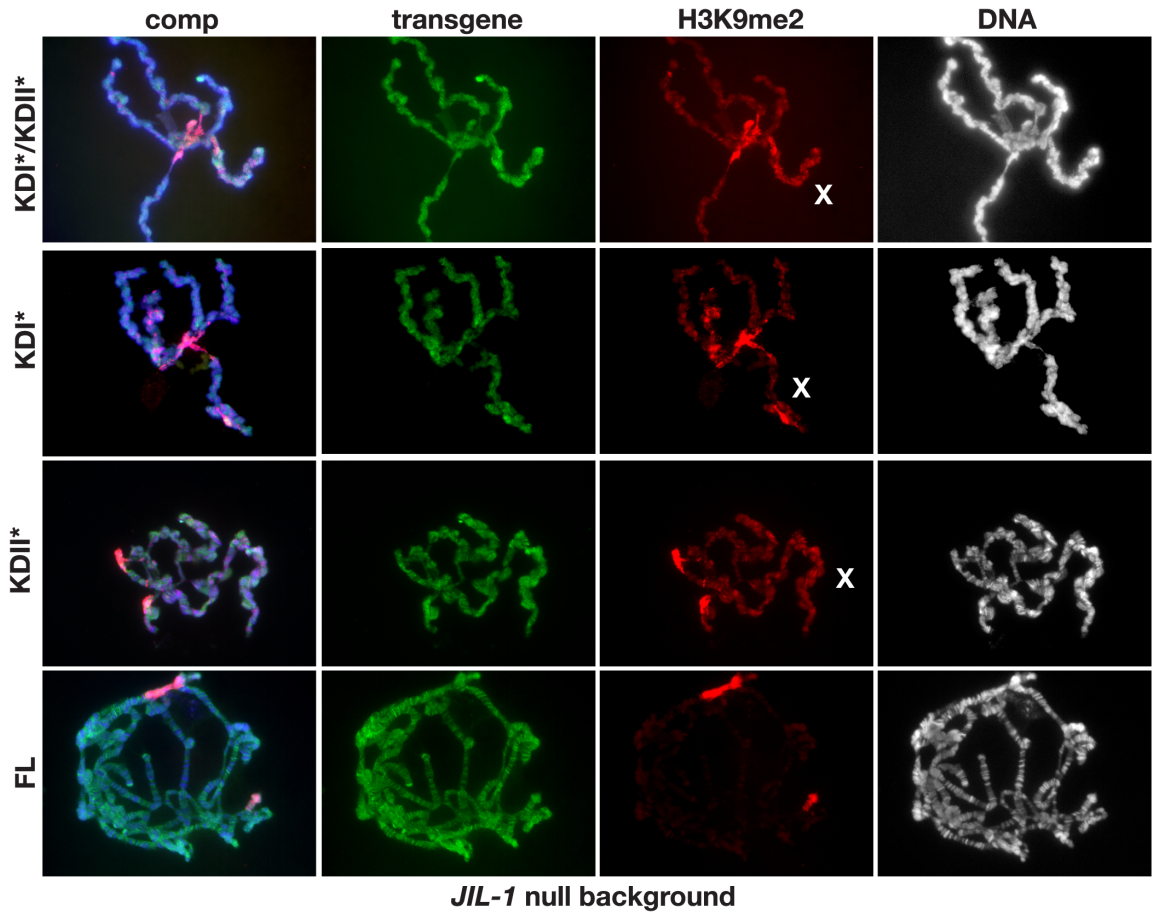

FIGURE 5. **Immunocytochemical analysis of polytene chromosome morphology and histone H3K9 dimethylation in *JIL-1* null larvae expressing JIL-1 "kinase dead" transgenes.** The panels show polytene chromosome squash preparations from *JIL-1* null (*z2/z2*) third instar larval salivary glands expressing the KDI*/KDII*, KDII*, KDI*, and FL, respectively. Protein localization (in green) was identified using JIL-1 antibody, histone H3K9 dimethylation (in red) was identified using H3K9me2 antibody, and DNA (in blue or gray) was labeled by Hoechst.

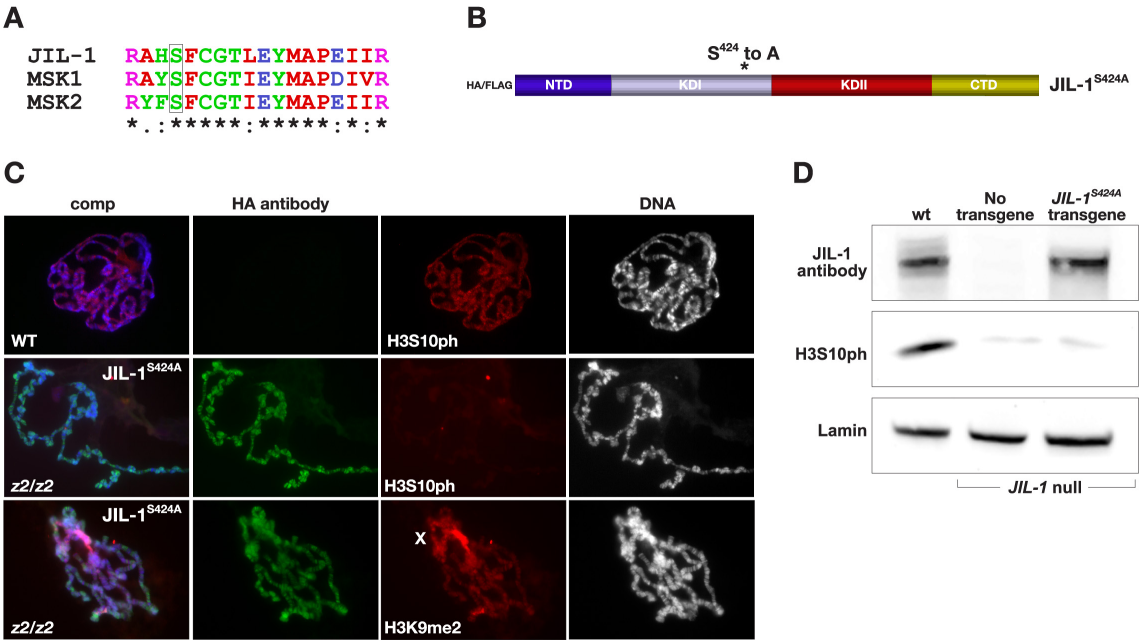

FIGURE 6. **Immunocytochemical and immunoblot analysis of a transgenic JIL-1^{S424A} point mutation construct expressed in a *JIL-1* null background.** (A) Alignment of the amino acid sequences flanking a conserved serine (box) in the first kinase domain of JIL-1 and human MSK1/2. (B) Diagram of the JIL-1 HA/FLAG-tagged JIL-1^{S424A} point mutation construct analyzed. (C) Polytene chromosome squash preparations from wild-type (WT) as well as *JIL-1* null (*z2/z2*) third instar larval salivary glands expressing the JIL-1^{S424A} construct. JIL-1^{S424A} localization (in green) was identified using HA antibody, histone H3K9 dimethylation (in red) was identified using H3K9me2 antibody, histone H3S10 phosphorylation (in red) was identified using H3S10ph antibody, and DNA (in blue or gray) was labeled by Hoechst. (D) Immunoblot labeled with H3S10ph antibody of protein extracts from salivary glands from wild type third instar larvae (wt), from *JIL-1* null salivary glands, and from *JIL-1* null salivary glands expressing the JIL-1^{S424A} construct. Endogenous JIL-1 and JIL-1^{S424A} construct expression were detected by JIL-1 antibody labeling. Labeling with Lamin antibody was used as a loading control.

Tables

Table1. Properties of JIL-1 constructs expressed in a *JIL-1*^{z2}/*JIL-1*^{z2} null background

construct	localization to chromatin	rescue of autosome morphology	H3S10 phosphorylation	H3K9me2 spreading	% rescue of adult viability[a] (n)
JIL-1-FL	yes	yes	yes	no	58.6% (644)
CTD	yes	yes	no	yes	13.6% (515)
DCTD	yes[b]	yes	yes	no	4.4% (591)
DNTD	yes	yes	no	yes	18.9% (428)
KD1*/KD2*	yes	no	no	yes	22.9% (447)
KD1*/KD2	yes	no	no	yes	14.3% (329)
KD1/KD2*	yes	no	no	yes	12.3% (568)
JIL-1^{S424A}	yes	partial	no	yes	14.7% (439)

[a]The rescue of adult viability in the *JIL-1* null mutant background by each contruct was calculated as described in Material and Methods. n indicates the total number of enclosed progeny in each experiment.
[b]Ectopic chromatin localization.

CHAPTER 4. GENOME-WIDE ANALYSIS OF REGULATION OF GENE EXPRESSION AND H3K9ME2 DISTRIBUTION BY JIL-1 KINASE MEDIATED HISTONE H3S10 PHOSPHORYLATION IN *DROSOPHILA*

A paper published in the *Nucleic Acid Research*

Weili Cai, Chao Wang, Yeran Li, Changfu Yao, Lu Shen, Sanzhen Liu, Xiaomin Bao, Patrick S. Schnable, Jack Girton, Jørgen Johansen and Kristen M. Johansen

Summary

In this study we have determined the genome-wide relationship of JIL-1 kinase mediated H3S10 phosphorylation with gene expression and the distribution of the epigenetic H3K9me2 mark. We show in wild-type salivary gland cells that the H3S10ph mark is predominantly enriched at active genes whereas the H3K9me2 mark largely is associated with inactive genes. Comparison of global transcription profiles in salivary glands from wild-type and *JIL-1* null mutant larvae revealed that the expression levels of 1539 genes changed at least two-fold in the mutant and that a substantial number (49%) of these genes were upregulated whereas 51% were downregulated. Furthermore, the results showed that downregulation of genes in the mutant was correlated with higher levels or acquisition of the H3K9me2 mark whereas upregulation of a gene was correlated with loss of or diminished H3K9 dimethylation. These results are compatible with a model where gene expression levels are modulated by the levels of the H3K9me2 mark independent of the state of the H3S10ph mark, which is not required for either transcription or gene activation to occur. Rather,

H3S10 phosphorylation functions to indirectly maintain active transcription by counteracting H3K9 dimethylation and gene silencing.

Introduction

The JIL-1 kinase localizes specifically to euchromatic interband regions of polytene chromosomes and is the kinase responsible for histone H3S10 phosphorylation at interphase in *Drosophila* (1,2). Genetic interaction assays with *JIL-1* hypomorphic and null allelic combinations demonstrated that JIL-1 can counterbalance the gene-silencing effect of the three major heterochromatin markers H3K9me2, Su(var)3-7, and HP1a on position-effect variegation and that in the absence of histone H3S10 phosphorylation these epigenetic marks spread to ectopic locations on the arms of polytene chromosomes (3-7). These observations suggested a model for a dynamic balance between euchromatin and heterochromatin (3,5,6,8), where the level of gene expression is determined by antagonistic functions of the euchromatic H3S10ph mark on the heterochromatic H3K9me2 mark. In strong support of this model Wang et al. (6,9) recently provided evidence that H3K9me2 levels at reporter genes inversely correlate with their levels of expression and that H3K9me2 levels in turn are regulated by H3S10 phosphorylation. Thus, taken together these findings suggest that a major function of JIL-1 mediated histone H3S10 phosphorylation is to maintain an active state of chromatin by counteracting H3K9 dimethylation and gene silencing (3,6,9,10). In an alternative scenario Corces and co-workers have proposed that JIL-1 and histone H3S10 phosphorylation are required for active transcription by the RNA polymerase II machinery (11-13). However, the

results of these studies have been controversial because it has been demonstrated that RNA polymerase II-mediated transcription occurs at robust levels in the absence of H3S10 phosphorylation in *Drosophila* (10,14,15).

In this study to explore the global interplay between the epigenetic H3S10ph and H3K9me2 chromatin modifications and gene expression, we conducted a genome-wide analysis of their enriched sites and combined it with an analysis of changes to the distribution of the H3K9me2 mark and of whole genome transcription level changes in the absence of H3S10 phosphorylation. In order to have the ability to specifically map and correlate the location of JIL-1 and H3K9me2 with the locations of the histone H3S10 phosphorylation mark, salivary gland cells from third instar larvae were analyzed. Salivary gland nuclei are all at interphase excluding contributions from mitotic histone H3S10 phosphorylation. We found that most of the identified JIL-1 binding peaks located at or near transcription start sites (TSS) whereas peaks for both H3S10ph and H3K9me2 enrichment were located around 600 bp downstream of the TSS. A comparison of the transcriptome profiles of salivary glands from wild type and *JIL-1* null mutants revealed that the expression levels of 1539 genes changed at least two-fold in the mutant. Interestingly, out of these genes the expression of 66% of normally active genes was repressed, whereas the expression of most normally inactive genes (77%) was activated. Furthermore, we show that in the absence of H3S10 phosphorylation the H3K9me2 mark redistributes and becomes upregulated on ectopic sites on the chromosome arms, especially on the X-chromosome, and that this H3K9me2 redistribution correlates with the activation

of silent genes and the repression of active genes. Taken together these results provide direct support for the model that H3S10 phosphorylation mainly facilitates gene expression of active genes by maintaining an open chromatin structure at promoter regions by counteracting H3K9 dimethylation.

Materials And Methods

Drosophila melanogaster stocks

Fly stocks were maintained according to standard protocols (16). Canton S. was used for wild type preparations. The *JIL-1*^{z2} allele is described in Wang et al. (2) and in Zhang et al. (17).

ChIP-Sequencing and data analysis

For ChIP-sequencing, 50 pairs of salivary glands per sample were dissected from third instar larvae and fixed for 15 minutes at room temperature in 1 ml of fixative (50 mM HEPES at pH 7.6, 100 mM NaCl, 0.1 mM EDTA at pH 8, 0.5 mM EGTA at pH 8, 2% formaldehyde). Preparation of chromatin for immunoprecipitation was performed as previously described (18). Mouse anti-JIL-1 mAb 5C9 (19), mouse anti-H3K9me2 mAb 1220 (Abcam), or rabbit anti-H3S10ph pAb (Cell Signaling or Active Motif) were used for immunoprecipitation. For each sample, 10% of the chromatin lysate was used as control input DNA, and 90% was immunoprecipitated with the antibody. DNA from the immunoprecipitated chromatin fragments was purified using a Wizard SV DNA purification kit (Promega).

Before sequencing the purified ChIP-enriched DNA fragments were selected on an agarose gel for fragments 200 bp in size, linkers were added, and the library was amplified by PCR. Each library was sequenced at the Iowa State University DNA facility by a Genome Analyser II next-generation sequencing platform (Illumina). All samples were processed using the standard 36 bp single-end protocol (Illumina). All reads were mapped to version 3 of the *Drosophila melanogaster* genome using Bowtie V0.12.7 (20) with the default settings and output to the SAM format. SAMtools V0.1.18 (21) and BEDtools V2.14.3 (22) were used to sort and transfer files. Enriched islands for JIL-1, H3S10ph and H3K9me2 (wild-type and $JIL\text{-}1^{Z2}$/ $JIL\text{-}1^{Z2}$) were identified using SICER V1.1 with 200 bp window size, 200 bp gap size, and an effective genome size of 72% of the *Drosophila* genome (23). Enriched islands with a false discovery rate (FDR) of 1% or less were considered to be valid. MACS V1.4 (24) was used to identify JIL-1 binding peaks with default settings and FDRs of 10% or less. Binding islands or the number of reads obtained in each genomic region scaled to the total number of reads were rendered in the integrated genome viewer (IGV 2.0). ChIP on chip profiles of Chromator were generated from data in Kc cells obtained by ModENCODE (25) and presented as average log2 signal ratio of IP over input. The ChIPpeakAnno bioconductor R package (26) was employed to annotate the binding sites to the nearest start of a gene and to map the distance to the nearest TSS. Density plots of the center of enriched binding islands relative to the distance from the TSS of nearby genes were made using SAS (SAS Institute Inc).

RNA-sequencing and data analysis

For RNA-sequencing total RNA from third instar salivary glands was isolated using the UltraClean Tissue and Cells RNA isolation Kit (Mo Bio). DNA was removed using the DNase I kit (Mo Bio). Two replicated samples of each Wild-type and *JIL-1*^{z2}/*JIL-1*^{z2} null mutant RNA were amplified and sequenced on an Illumina Hiseq2000 at the Iowa State University DNA facility using a paired-end protocol. Low quality nucleotides were removed from raw reads using Data2Bio's trimming script (27). GSNAP (Genomic Short-read Nucleotide Alignment Program, version 2013-10-12) (28), which allows for intron-spanning alignments, was used to map trimmed reads to the reference genome (BDGP 5.72/dm3 June 2013). Reads with one unique best match in the reference genome (BDGP 5.72/dm3 June 2013) with ≤2 mismatches every 75 bp were used for all subsequent analyses. The read depth of each gene was computed based on the coordinates of mapped reads and the annotated locations of genes in the reference genome (BDGP 5.72/dm3 June 2013). Reads per kilobase of exons per million uniquely mapped reads (RPKM) values were calculated as in Mortazavi et al. (29).

For identification of genes with different expression in the *JIL-1* mutant background the log-scale 75th percentile of library size normalization method was used to normalize wild-type and mutant RNA-Seq reads (30). The normalized reads were counted by HTseq(v0.5.4). The QuasiSeq (R package) was used to identify differentially expressed genes by negative binomial quasi-likelihood estimation (31). Genes were considered differentially expressed between wild-

type and the mutant if they exhibited a greater than 2 fold change in expression and an FDR smaller than 0.05. Scatter plot representations of gene expression changes between wild-type and *JIL-1* null mutant salivary gland cells as well as regression analysis were performed using SAS (SAS Institute Inc). Gene Ontology (GO) term categories for genes identified as down- or up-regulated in *JIL-1* null mutant versus wild-type salivary glands were identified by DAVID (32) in Level 5 of biological process and molecular function. In addition, boxplots, bar charts, and pie charts were made used using the ggplot2 R package (33) and statistical analysis was performed with R (v3.0.1).

Chromatin immunoprecipitation and qPCR

ChIP experiments were performed as previously described (6,18). In short, for ChIP experiments, 50 pairs of salivary glands per sample were dissected from third instar larvae and fixed for 15 minutes at room temperature in 1 ml of fixative (50 mM HEPES at pH 7.6, 100 mM NaCl, 0.1 mM EDTA at pH 8, 0.5 mM EGTA at pH 8, 2% formaldehyde). Mouse anti-JIL-1 mAb 5C9 (19), anti-H3K9me2 (Abcam), anti-GST mAb 8C7 (34), anti-H3S10ph (Cell Signaling, Active Motif) or purified rabbit IgG(Sigma) were used for immunoprecipitation. For each sample, the chromatin lysate was divided into equal amounts and immunoprecipitated with experimental and control antibody, respectively. DNA from the immunoprecipitated chromatin fragments (average length, 500 bp) was purified using a Wizard SV DNA purification kit (Promega).

Quantitative PCR was carried out using Brilliant® II SYBR Green QPCR Master Mix (STRATAGENE) in conjunction with an Mx4000 (STRATAGENE)

PCR machine. The primers used for the various qPCR experiments are listed in Supplementary Table 1. Cycling parameters were 10 min at 95°C, followed by 40 cycles of 30 sec at 95°C, 30 sec at 55°C, and 30 sec at 72°C. Fluorescence intensities were plotted against the number of cycles using an algorithm provided by Stratagene. Template levels were quantified using a calibration curve based on dilution of concentrated DNA. For each experimental condition the relative enrichment was normalized to the corresponding control immunoprecipitation from the same chromatin lysate.

Immunohistochemistry

Polytene chromosome squash preparations were performed as in Cai et al. (35) using a 5 minute fixation protocol and double labeled with JIL-1 mAb 5C9 (19) and rabbit anti-histone H3K9me2 (Millipore). DNA was counterstained by Hoechst 33258 (Molecular Probes) in PBS. The appropriate species- and isotype- specific TRITC-, and FITC- conjugated secondary antibodies (Cappel/ICN, Southern Biotech) were used (1:200 dilution). The final preparations were mounted in 90% glycerol containing 0.5% n-propyl gallate. The preparations were examined using epifluorescence optics on a Zeiss Axioskop microscope and images were captured and digitized using a cooled Spot CCD camera. Images were imported into Photoshop where they were pseudocolored, image processed, and merged. In some images non-linear adjustments were made to the channel with Hoechst labeling for optimal visualization of chromosomes.

Modeling of JIL-1

The structure of JIL-1 was modeled with the I-TASSER protein prediction server (36,37) and compared to the crystal structure of a nucleosome (PDB ID: 1AOI). I-TASSER generates models of proteins by excising continuous fragments from Local Meta-Threading-Server multiple-threading alignments and then reassembling them using replica-exchange Monte Carlo simulations (38). The comparison and visualization between the model of JIL-1 and the nucleosome was processed and rendered by PyMOL.

Data Access

The ChIP-Seq and RNA-Seq data of this study have been deposited in the NCBI Gene Expression Omnibus and is accessible for review purposes at: http://www.ncbi.nlm.nih.gov/geo/query/acc.cgi?token=jbkffaicascisfa&acc=GSE41047

Results

Mapping the genome-wide distribution of JIL-1, H3S10ph, and H3K9me2 in salivary gland cells

All DNA and RNA samples analyzed were from post-mitotic third instar larval salivary glands that included both sexes and issues of JIL-1's and H3S10 phosphorylation's role in dosage compensation of the X-chromosome were not addressed in this study. For comparisons of gene transcription and H3K9me2 distribution in the absence of JIL-1 and H3S10 phosphorylation with wild-type we analyzed DNA and RNA from salivary glands of *JIL-1*^{z2}/*JIL-1*^{z2} homozygous larvae. *JIL-1*^{z2} is a true null allele generated by P-element mobilization (2). The global transcription profiles were generated by analysis of two independent RNA-

Seq experiments. Based on the formula of Mortazavi et al. (29) we calculated that in salivary glands one read per kilobase of exons per million uniquely mapped reads (RPKM) corresponded to approximately one transcript per cell. Thus, genes with an RPKM of one or more were considered active, otherwise they were categorized as inactive. We further classified the active genes into three separate groups with low, moderate, or high expression levels reflected by RPKMs of from 1-5, >5-30, or >30, respectively. For ChIP-Seq analysis of JIL-1 genomic binding sites we used a previously characterized and highly specific mAb 5C9 (19) and conducted two independent experiments. Enriched chromatin binding sites were identified using the SICER algorithm (23) (Fig. 1A). The resulting two data sets were highly correlated (Supplemental Fig. S1) and we identified 2819 genes associated with binding sites enriched for JIL-1 present in both data sets that were used for the following analysis. For ChIP-Seq analysis of the genome-wide distribution of the H3S10ph mark we used two previously validated antibodies (6,9) from Cell Signaling (CS) and Active Motif (AM), respectively. As illustrated in Supplemental Fig. S1 the two data sets for these antibodies were strongly correlated and we identified 2948 genes enriched for H3S10ph present in both data sets that were used for the subsequent analysis. For analysis of the H3K9me2 mark we used the mAb 1220 (Abcam) verified for ChIP-analysis by ModENCODE (25) as well as by Wang et al. (6,9) and determined its global distribution in both wild-type and in the *JIL-1* null mutant background. Based on two independent ChIP-Seq experiments for each condition we identified 833 genes enriched for H3K9me2 in both data sets for

wild-type and 488 genes enriched for H3K9me2 in both data sets from the *JIL-1* null background (Supplemental Fig. S1). To further validate our RNA-Seq data we confirmed selected genes with qPCR assays (Supplemental Fig. S2).

Genome-wide DNA-enrichment profiles for JIL-1, H3S10ph, and H3K9me2

In order to determine the relative distribution of JIL-1 and the H3S10ph and H3K9me2 marks in salivary gland cells we generated high-resolution genome-wide DNA-enrichment profiles as exemplified in Fig. 1A and Supplemental Fig. S3. In addition, we compared these profiles to that of Chromator obtained by ChIP on chip analysis by ModENCODE in Kc cells (25). A caveat to this analysis is that the data are from different cells and tissues. Chromator is a chromodomain containing protein (34,39) that is a known binding partner of JIL-1 that co-localizes with JIL-1 at interband regions in immunolabeled polytene salivary gland squash preparations (40). To further characterize the enrichment in and around genes we plotted the distribution of the middle position of the enriched islands (clusters of enriched windows) determined by SICER (23) relative to transcription start sites (TSS) of genes (Fig. 1B). As illustrated in Fig. 1B genome-wide distance correlation revealed that the majority of the identified JIL-1 enriched islands were centered in close proximity to the TSS within ±500 bp and that the peak was aligned near 0 bp. Interestingly, the distribution of Chromator enriched islands with respect to the TSS was nearly identical to that of JIL-1 (Fig. 1B). Furthermore, analysis of discrete binding peaks of JIL-1 determined by the MACS peak-finding algorithm (24) revealed that they were highly correlated with Chromator binding peaks and located preferentially to the

5'-end of genes (Fig. 1C). These data suggest that JIL-1 and Chromator share the same specific binding sites although it has been demonstrated that neither depends on the other for its binding (40). Although the majority of JIL-1 binding peaks map in the proximity of the TSS we also found the presence of many binding regions at the level of exons, introns, and the 3'-end of genes (Fig. 1A).

Although H3S10ph enrichment was highly correlated with that of JIL-1 (Fig. 1A and Supplemental Fig. S1), the profile of H3S10ph was markedly different from that of JIL-1 around the TSS (Fig. 1B). H3S10ph's distribution was much broader and the peak enrichment was shifted to about 600 bp downstream of the TSS. This suggests that JIL-1 may not phosphorylate histone H3 at the nucleosome to which it is bound. To explore this possibility we modeled the 3D-structure of JIL-1 using the I-TASSER structure prediction program (37) and compared it to the nucleosome crystal structure (41). As illustrated in Supplemental Fig. S4 considering that JIL-1 is known to bind the tail of H3 by the end of its carboxy-terminal domain (42) and that its folded structure is larger than a nucleosome, it is likely to have the capacity to phosphorylate histone H3 of one or more nucleosomes some distance away from its actual binding site depending on the state of higher order nucleosome packaging. Thus, as indicated by the present data the distribution of JIL-1 and H3S10 phosphorylation may not necessarily be coincident. Interestingly, the distribution of H3K9me2 binding around the TSS closely mirrored that of H3S10ph (Fig. 1B) indicating that these two epigenetic modifications may occur in similar genomic contexts.

H3S10 phosphorylation is enriched at active genes and correlated with enhanced gene expression

JIL-1 mediated H3S10 phosphorylation has been proposed to maintain an active state of chromatin (43). Consistent with this hypothesis we found that enrichment of JIL-1 and the H3S10ph mark predominantly were associated with active genes (79% and 67%, respectively) (Fig. 2A). In contrast, enrichment of the H3K9me2 mark had a more pronounced association with inactive genes (47%) (Fig. 2A). However, it should be noted that JIL-1 and the H3S10ph mark were also enriched at many inactive genes (21% and 33%, respectively) whereas the enrichment of the H3K9me2 mark in many cases was associated with active genes (53%) (Fig. 2A). Thus, to further explore the correlation of gene expression's dependence on the presence of the H3S10ph and H3K9me2 marks we determined the average gene expression of genes enriched for the H3S10ph or H3K9me2 mark only and genes enriched for both marks. As illustrated in Fig. 2B the median gene expression for these groups of genes were significantly different from each other with the highest expression of genes enriched for the H3S10ph mark only and lowest expression of genes enriched with the H3K9me2 mark only, whereas gene expression for genes enriched for both marks were intermediate. We further compared the relative proportions of high expression, moderate expression, low expression, and inactive genes associated with enriched levels of the H3S10ph or H3K9me2 mark only and genes enriched for both marks (Fig. 2C). The results show that the proportion of both high, moderate, and low expression genes were greater when associated with enriched levels of the H3S10ph mark only and conversely that the proportion of

inactive genes increased with enriched levels of the H3K9me2 mark only. The relative proportion of high, moderate, and low expressing genes was intermediate between genes with enrichment for both marks compared to the distribution of these classes of genes with single marks (Fig. 2C). Thus, taken together these results suggest that at a genome-wide level the enrichment for the H3S10ph mark is directly correlated with enhanced gene expression.

Loss of JIL-1 and H3S10 phosphorylation lead to both gene up- and downregulation

In order to determine the changes in gene transcription in the absence of H3S10 phosphorylation we compared global transcription profiles in salivary glands in two biological replicates from wild-type and *JIL-1*^{z2}/*JIL-1*^{z2} homozygous null larvae, respectively. The replicate determinations were highly correlated with Pearson's coefficients (R^2) of 0.977 for the two wild-type samples and 0.998 for the two samples from *JIL-1* null larvae. The results showed that out of nearly 15,000 genes analyzed, the expression levels of 1539 genes changed at least two-fold and with an FDR smaller than 0.05. Interestingly, 51% of these genes were downregulated whereas 49% showed increased expression levels in the *JIL-1* null mutant background. This is illustrated in the scatterplot in Fig. 3A where each dot represents the changes in the expression level of each individual gene and in the box-plot in Fig. 3B. We further plotted the changes in gene expression levels of genes that were classified as active or inactive in wild-type salivary glands. As shown in the box-plot in Fig. 3C there was a significant difference in the expression changes between the two groups of genes. Most inactive genes had increased expression in the mutant background whereas

active genes on average had a modest decrease. However, when active genes were further divided into groups with low, moderate, and high expression there was a clear trend that the higher the wild-type expression levels of a gene the more its expression levels were decreased in the mutant background (Fig. 3D). These data suggest in general that active genes become repressed but that many hitherto inactive genes become activated in the absence of H3S10 phosphorylation.

We next analyzed the up- and downregulated genes in terms of their GO categories (Fig. 3E). Strikingly, the results indicate that the downregulated set of genes in the mutant is enriched in categories related to salivary gland function and development whereas the upregulated list is enriched in DNA repair, cellular response to stress, and RNA processing and metabolism categories. That genes in salivary gland and tissue development specific pathways were particularly affected by downregulation in the mutant suggests that H3S10 phosphorylation may play a key role in keeping tissue and developmentally stage specific genes transcriptionally active.

H3K9me2 redistribution in the absence of H3S10 phosphorylation correlates with activation of silent genes and repression of active genes

One of the consequences of the absence of H3S10 phosphorylation is a redistribution of the H3K9me2 mark from pericentric heterochromatin to the euchromatic regions of the chromosome arms (3-7). This is illustrated by the H3K9me2 immunolabeling of polytene squash preparations from wild-type and *JIL-1* null mutant salivary glands in Fig. 4A with the redistribution especially prominent on the X-chromosome of both males and females (3). Thus, to further

investigate this redistribution on a genome-wide level we generated maps of H3K9me2 binding by plotting normalized read numbers in 200 bp bins across the genome from wild-type and *JIL-1* null salivary glands. Fig. 4B shows an example of such maps comparing wild-type and *JIL-1* mutant X-chromosomes. The results show that in the *JIL-1* null mutant background the levels of H3K9me2 on the chromosome arms were markedly increased and that enriched levels occurred at sites previously not occupied by significant levels of the H3K9me2 mark. Interestingly, although the H3K9me2 mark was enriched on the X-chromosome compared to the autosomes, overall gene expression levels were not statistically different (Fig. 4C).

The study of Wang et al. (9) of gene expression of the *white* locus provided evidence that H3K9me2 levels at the *white* gene directly correlated with its level of expression and that the H3K9me2 levels in turn were regulated by H3S10 phosphorylation. Based on these findings we reasoned that in the absence of H3S10 phosphorylation gene repression should correlate with increased H3K9me2 binding to the gene, whereas gene activation should be correlated with a loss or decreased H3K9me2 binding. To explore this hypothesis we plotted the expression of all moderate and high expression genes in our data set without enriched levels of H3K9me2 that acquired the H3K9me2 mark in the *JIL-1* mutant. As illustrated by the box plots in Fig. 5A, for 94 such genes there was a significant decrease in their average levels of expression. To further validate these findings we performed ChIP-assays as in Wang et al. (6,9) for five randomly selected genes among the genes analyzed above. Chromatin was

immunoprecipitated (ip) from wild-type or *JIL-1* null mutant larval salivary glands using rabbit anti-H3S10ph antibody or purified rabbit IgG antibody (negative control) or mAbs to H3K9me2 or GST (negative control). Primers specific for each of the selected genes were used to amplify the precipitated material. Experiments were done in triplicate and relative enrichment of DNA from the H3S10ph and H3K9me2 ips were normalized to the corresponding control antibody ips performed in tandem for each experimental sample. As illustrated in Fig. 5B, at all five genes the relative enrichment of H3S10ph in the mutant was reduced to background levels whereas there was a significant increase of from 2 to 7 fold of the enrichment of the H3K9me2 mark. We next plotted the expression of all inactive and low expression genes in our data set that lost the H3K9me2 mark in the *JIL-1* mutant. The box plots in Fig. 6A show that for 69 such genes there was a significant increase in their average levels of expression. As above we validated these findings by performing ChIP-assays for five randomly selected genes among the genes analyzed. The results show that at all five genes there was a significant decrease of from 2 to 6 fold of the enrichment of the H3K9me2 mark (Fig. 6B). Furthermore, the results confirm that in this class of inactive genes there were very low wild-type levels of H3S10ph. Taken together these findings suggest that H3S10 phosphorylation modulates H3K9 dimethylation and that H3K9me2 redistribution in the absence of H3S10 phosphorylation correlates with activation of silent genes that lose the H3K9me2 mark and repression of active genes that acquire the H3K9me2 mark.

Discussion

In this study we have determined the relationship of JIL-1 kinase mediated H3S10 phosphorylation with gene expression and the distribution of the epigenetic H3K9me2 mark. We show in wild-type salivary gland cells that the H3S10ph mark is predominantly enriched at active genes whereas the H3K9me2 mark largely is associated with inactive genes. Furthermore, our data demonstrate that discrete binding peaks of JIL-1 are located preferentially to the 5'-end of genes near the TSS and that these peaks are coincident with binding peaks for the chromodomain protein, Chromator, a known binding partner for JIL-1 (40). This distribution of JIL-1 around the TSS is similar to that obtained by ChIP-Seq by Kellner et al. (13) in Kc cells but differs from that reported by Regnard et al. (10) using ChIP-chip analysis on custom tiling arrays in S2 cells. These latter workers found JIL-1 to be more or less equally distributed along the entire length of genes; however, this result may be a consequence of using lower affinity polyclonal antibodies combined with the lower resolution ChIP-chip approach. Interestingly, we found that although the enrichment profile of H3S10ph was highly correlated with that of JIL-1, the two profiles were not identical. The distribution of the H3S10ph mark was much broader and peak enriched regions were shifted about 600 bp downstream of the TSS. Modeling of the 3D-structure of JIL-1 relative to nucleosome structure suggested that a reason for this lack of overlap is that JIL-1 may have the capacity to phosphorylate the tail of H3 of one or more nucleosomes some distance away

from its actual binding site depending on the state of higher order nucleosome packaging.

Comparison of global transcription profiles in salivary glands from wild-type and *JIL-1* null mutant larvae revealed that of the nearly 15,000 genes analyzed the expression levels of 1539 genes changed at least two-fold in the mutant. Surprisingly, among these genes almost as many (49%) increased their expression as were downregulated (51%). This raised the question whether certain classes of genes were preferentially up- or downregulated and further analysis suggested that in general active genes became repressed, whereas hitherto inactive genes became activated in the absence of H3S10 phosphorylation. Furthermore, the results showed that downregulation of genes in the mutant was correlated with higher levels or acquisition of the H3K9me2 mark whereas upregulation of a gene was correlated with loss of or diminished H3K9 dimethylation. These findings directly demonstrate that H3S10 phosphorylation is not required for transcription or gene activation in *Drosophila* as proposed by Corces and colleagues (11-13). This conclusion is further supported by recent experiments by Wang et al. (9) analyzing *white* gene expression where levels of the H3S10ph mark can be manipulated and correlated with the resulting levels of the H3K9me2 mark using ChIP-assays. In wild-type there are moderate levels of the H3S10ph mark and low levels of the epigenetic H3K9me2 mark at the *white* gene resulting in its normal expression. However, in the w^{m4} allele heterochromatic factors can spread across the inversion breakpoint (5,6,43,44) leading to high levels of H3K9me2 at the *white*

gene and silencing of gene expression. Interestingly, Wang et al. (9) demonstrated that this increase in H3K9me2 level can be prevented by ectopic H3S10 phosphorylation at the *white* gene restoring gene expression. In contrast, in the absence of H3S10 phosphorylation as it occurs in strong *JIL-1* hypomorphic mutant backgrounds there is a redistribution of heterochromatic factors to ectopic chromosome sites resulting in reduced levels of these factors at the pericentric heterochromatin (3). This leads to less heterochromatic spreading and lower levels of H3K9me2 at the *white* gene in the w^{m4} inversion, thus allowing for increased *white* gene expression (9). Thus, taken together these results are compatible with a model (Fig. 7) where gene expression levels are directly correlated with the levels of the H3K9me2 mark independent of the state of the H3S10ph mark, which is not required for either transcription or gene activation to occur. However, H3S10 phosphorylation functions to indirectly regulate transcription by counteracting H3K9 dimethylation and gene silencing in a finely tuned balance (3,5,6,8).

That genes in GO categories for salivary gland specific pathways were particularly affected by downregulation in a *JIL-1* mutant background suggest that H3S10 phosphorylation may serve to keep genes transcriptionally active in a tissue and/or developmentally stage specific context. How JIL-1 and H3S10 phosphorylation get targeted to specific sets of genes is not known. However, it has been suggested as a general model that JIL-1 targeting to active chromatin may be facilitated by or dependent on the presence of the H3K36me2 and H4K16ac marks (10). Interestingly, the GO categories for genes becoming

activated or upregulated in the absence of H3S10 phosphorylation were enriched in DNA repair, DNA and RNA metabolism, and cellular response to stress pathways. Upregulation of such genes would be consistent with a cellular attempt to compensate for the general downregulation of active genes and to the gross perturbation of chromatin structure occurring in *JIL-1* null mutant backgrounds (2,45). If this represents a specific response to alterations in the mutant it implies activation of unknown gene induction pathways independent of H3S10 phosphorylation. However, an alternative scenario is that when the H3S10ph mark, which normally serves to limit heterochromatic spreading, is lost in the *JIL-1* mutant, the H3K9me2 silencing mark can now disperse away from previously repressed locations, resulting in transcriptional activation of the now unmasked genes.

In summary, the findings of this study indicate that a major functional role of JIL-1 mediated H3S10 phosphorylation is to maintain active gene expression by serving as a protective epigenetic mark counteracting H3K9 dimethylation and gene silencing. This suggests that different gene expression profiles are regulated by strategic deployment of silencing marks within the genome, and that H3S10 phosphorylation can be an effective means of counteracting silencing effects. This may also be relevant in other organisms where H3S10ph is implicated in the rapid yet transient induction of promoters in response to various inducers (46,47).

Acknowledgements

We thank Dr. D. Nettleton and members of the laboratory for discussion and advice. We also wish to acknowledge Mr. Atrez Norwood and Mr. Cheng-Ting Yeh for technical assistance.

References

1. Jin, Y., Wang, Y., Walker, D.L., Dong, H., Conley, C., Johansen, J. and Johansen, K.M. (1999) JIL-1: a novel chromosomal kinase implicated in transcriptional regulation in *Drosophila*. *Mol. Cell* **4,** 129-135.
2. Wang, Y., Zhang, W., Jin, Y., Johansen, J. and Johansen, K.M. (2001) The JIL-1 tandem kinase mediates histone H3 phosphorylation and is required for maintenance of chromatin structure in *Drosophila*. *Cell* **105,** 433-443.
3. Zhang, W., Deng, H., Bao, X., Lerach, S., Girton, J., Johansen, J. and Johansen, K.M. (2006) The JIL-1 histone H3S10 kinase regulates dimethyl H3K9 modifications and heterochromatic spreading in *Drosophila*. *Development* **133,** 229-235.
4. Deng, H., Bao, X., Zhang, W., Girton, J., Johansen, J. and Johansen, K.M. (2007) Reduced levels of Su(var)3-9 but not Su(var)2-5 (HP1) counteract the effects on chromatin structure and viability in loss-of-function mutants of the JIL-1 histone H3S10 kinase. *Genetics* **177,** 79-87.
5. Deng, H., Cai, W., Wang, C., Lerach, S., Delattre, M., Girton, J., Johansen, J. and Johansen, K.M. (2010) *JIL-1* and *Su(var)3-7* interact genetically and counterbalance each others' effect on position effect variegation in Drosophila. *Genetics* **185,** 1183-1192.
6. Wang, C., Cai, W., Li, Y., Deng, H., Bao, X., Girton, J., Johansen, J. and Johansen, K.M. (2011) The epigenetic H3S10 phosphorylation mark is

required for counteracting heterochromatic spreading and gene silencing in *Drosophila melanogaster*. *J. Cell Sci.* **124,** 4309-4317.

7. Wang, C., Girton, J., Johansen, J., Johansen and K.M. (2011) A balance between euchromatic (JIL-1) and heterochromatic (SU(VAR)2-5 and SU(VAR)3-9) factors regulates position-effect variegation in Drosophila. *Genetics* **188,** 745-748.
8. Ebert, A., Schotta, G., Lein, S., Kubicek, S., Krauss, V., Jenuwein, T. and Reuter, G. (2004) *Su(var)* genes regulate the balance between euchromatin and heterochromatin in *Drosophila*. *Genes Dev.* **18,** 2973-2983.
9. Wang, C., Cai, W., L,i Y., Girton, J., Johansen, J. and Johansen, K.M. (2012) H3S10 phosphorylation by the JIL-1 kinase regulates H3K9 dimethylation and gene expression at the *white* locus in *Drosophila. Fly* **6,** 1-5.
10. Regnard, C., Straub, T., Mitterweger, A., Dahlsveen, I.K., Fabian, V. and Becker, P.B. (2011) Global analysis of the relationship between JIL-1 kinase and transcription. *PLoS Genetics* **7,** e1001327.
11. Ivaldi, M.S., Karam, C.S. and Corces, V.G. (2007) Phosphorylation of histone H3 at Ser10 facilitates RNA polymerase II release from promoter-proximal pausing in *Drosophila*. *Genes Dev.* **21,** 2818-2831.
12. Karam, C.S., Kellner, W.A., Takenada, N., Clemmons, A.W. and Corces, V.G. (2010) 14-3-3 mediates histone cross-talk during transcription elongation in *Drosophila. PLoS Genetics* **6,** e1000975.
13. Kellner, W.A., Ramos, E., Bortle, K.V., Takenada, N. and Corces, V.G. (2012) Genome-wide phosphoacetylation of histone H3 at *Drosophila* enhancers and promoters. *Genome Res.* **22,** 1081-1088.
14. Wang, C., Yao, C., Li, Y., Cai, W., Girton, J., Johansen, J. and Johansen, K.M. (2012) Evidence against a role for the JIL-1 kinase in H3S28 phosphorylation and 14-3-3 recruitment to active genes in *Drosophila. PLoS ONE* **8,** e62484.
15. Cai, W., Bao, X., Deng, H., Jin, Y., Girton, J., Johansen, J. and Johansen,

K.M. (2008) RNA polymerase II-mediated transcription at active loci does not require histone H3S10 phosphorylation in *Drosophila*. *Development* **135,** 2917-2925.

16. Roberts, D.B. (1998) *Drosophila*: A Practical Approach, 2nd ed, IRL Press, Oxford, UK.
17. Zhang, W., Jin, Y., Ji, Y., Girton, J., Johansen, J. and Johansen, K.M. (2003) Genetic and phenotypic analysis of alleles of the Drosophila chromosomal JIL-1 kinase reveals a functional requirement at multiple developmental stages. *Genetics* **165,** 1341-1354.
18. Legube, G., McWeeney, S.K., Lercher, M.J. and Akhtar, A. (2006) X-chromosome-wide profiling of MSL-1 distribution and dosage compensation in *Drosophila*. *Genes Dev.* **20,** 871-883.
19. Jin, Y., Wang, Y., Johansen, J. and Johansen, K.M. (2000) JIL-1, a chromosomal kinase implicated in regulation of chromatin structure, associates with the MSL dosage compensation complex. *J. Cell Biol.* **149,** 1005-1010.
20. Langmead, B., Trapnell, C., Pop, M. and Salzberg, S.L. (2009) Ultrafast and memory-efficient alignment of short DNA sequences to the human genome. *Genome Biol.* **10,** R25.
21. Li, H., Handsaker, B., Wysoker, A., Fennell, T., Ruan, J., Homer, N., Marth, G., Abecasis, G. and Durbin, R. (2009) The Sequence Alignment/Map format and SAMtools. *Bioinformatics* **25,** 2078-2079.
22. Quinlan, A.R. and Hall, I.M. (2010) BEDTools: a flexible suite of utilities for comparing genomic features. *Bioinformatics* , 841-842.
23. Zang, C., Schones, D.E., Zeng, C., Cui, K., Zhao, K. and Peng, W. (2009) A clustering approach for identification of enriched domains from histone modification ChIP-Seq data. *Bioinformatics* **25,** 1952-1958.
24. Zhang, Y., Liu, T., Meyer, C.A., Eeckhoute, J., Johnson, D.S., Bernstein, B.E., Nusbaum, C., Myers, R.M., Brown, M., Li, W. and Liu, X.S. (2008) Model-based analysis of ChIP-Seq(MACS). *Genome Biol.* **9,** R137.
25. Celniker, S.E., Dillon, L.A., Gerstein, M.B., Gunsalus, K.C., Henikoff, S.,

Karpen, G.H., Kellis, M., Lai, E.C., Lieb, J.D., MacAlpine, D.M., Micklem, G., Piano, F., Snyder, M., Stein, L., White, K.P., Waterston, R.H. and ModENCODE Consortium. (2009) Unlocking the secrets of the genome. *Nature* **459,** 927-930.

26. Zhu, L.J., Gazin, C., Lawson, N.D., Pagès, H., Lin, S.M., Lapointe, D.S. and Green, M.R. (2010) ChIPpeakAnno: a Bioconductor package to annotate ChIP-seq and ChIP-chip data. *BMC Bioinformatics* **11,** 237.
27. Liu, S., Yeh, C.T., Tang, H.M., Nettleton, D. and Schnable, P.S. (2012) Gene mapping via bulked segregant RNA-Seq (BSR-Seq). *PLoS ONE* **7,** e36406.
28. Wu, T. and Nacu, S. (2010) Fast and SNP-tolerant detection of complex variants and splicing in short reads. *Bioinformatics* **26,** 873-881.
29. Mortazavi, A., Williams, B.A., McCue, K., Schaeffer, L. and Wold, B. (2008) Mapping and quantifying mammalian transcriptomes by RNA-Seq. *Nat. Methods* **5,** 621-628.
30. Bullard, J.H., Purdom, E., Hansen, K.D. and Dudoit, S. (2010) Evaluation of statistical methods for normalization and differential expression in mRNA-Seq experiments. *BMC Bioinformatics* **11,** 94.
31. Lund, S.P., Nettleton, D., McCarthy, D.J. and Smyth, G.K. (2012) *Stat. Appl. Genet, Mol. Biol.* **11,** 1826.
32. Huang da, W., Sherman, B.T. and Lempicki, R.A. (2009) Systematic and integrative analysis of large gene lists using DAVID bioinformatics resources. *Nature Protocols* **4,** 44–57.
33. Wickham, H. (2009) *ggplot2: Elegant Graphics for Data Analysis.* Springer Press, Heidelberg, Germany.
34. Rath, U., Wang, D., Ding, Y., Xu, Y.-Z., Qi, H., Blacketer, M.J., Girton, J., Johansen, J. and Johansen, K.M. (2004) Chromator, a novel and essential chromodomain protein interacts directly with the putative spindle matrix protein Skeletor. *J. Cell. Biochem.* **93,** 1033-1047.
35. Cai, W., Jin, Y., Girton, J., Johansen, J. and Johansen, K.M. (2010) Preparation of polytene chromosome squashes for antibody labeling. *J Vis*

Exp http://www.jove.com/index/Details.stp?ID=1748.

36. Zhang, Y. (2007) Template-based modeling and free modeling by I-TASSER in CASP7. *Proteins* **68,** 108-117
37. Roy, A., Kucukural, A. and Zhang, Y. (2010) I-TASSER: a unified platform for automated protein structure and function prediction. *Nature Protocols* **5,** 725-738
38. Zhang, Y. (2008) Progress and challenges in protein structure prediction. *Curr. Opin. Struct. Biol.* **18,** 342–348.
39. Yao, C., Ding, Y., Cai, W., Wang, C., Girton, J., Johansen, K.M. and Johansen, J. (2012) The chromodomain-containing NH_2-terminus of Chromator interacts with histone H1 and is required for correct targeting to chromatin. *Chromosoma* **121,** 209-220.
40. Rath, U., Ding, Y., Deng, H., Qi, H., Bao, X., Zhang, W., Girton, J., Johansen, J. and Johansen, K.M. (2006) The chromodomain protein, Chromator, interacts with JIL-1 kinase and regulates the structure of *Drosophila* polytene chromosomes. *J. Cell Sci.* **11,** 2332-2341.
41. Luger, K., Mader, A.W., Richmond, R.K., Sargent, D.F. and Richmond, T.J. (1997) Crystal structure of the nucleosome core particle at 2.8 Å resolution. *Nature* **389,** 251-260.
42. Bao, X., Cai, W., Deng, H., Zhang, W., Krencik, R., Girton, J., Johansen, J. and Johansen, K.M. (2008) The COOH-terminal domain of the JIL-1 histone H3S10 kinase interacts with histone H3 and is required for correct targeting to chromatin. *J. Biol. Chem.* **283,** 32741-32750.
43. Johansen, K.M. and Johansen, J. (2006) Regulation of chromatin structure by histone H3S10 phosphorylation. *Chromosome Res.* **14,** 393-404.
44. Lerach, S., Zhang, W., Bao, X., Deng, H., Girton, J., Johansen, J. and Johansen, K.M. (2006) Loss-of-function alleles of the JIL-1 kinase are strong suppressors of position effect variegation of the w^{m4} allele in *Drosophila*. *Genetics* **173,** 2403-2406.

45. Deng, H., Zhang, W., Bao, X., Martin, J.N., Girton, J., Johansen, J., Johansen, K.M. (2005) The JIL-1 kinase regulates the structure of *Drosophila* polytene chromosomes. *Chromosoma* **114,** 173-182.

46. Winter, S., Simboeck, E., Fischle, W., Zupkovitz, G., Dohnal, I. and Berger, S.L. (2008) 14-3-3 proteins recognize a histone code at histone H3 and are required for transcriptional activation. *EMBO J.* **27,** 88-99.

47. Zippo, A., Serafini, R., Rocchigiani, M., Pennacchini, A., Krepelova, A. and Oliviero, S. (2009) Histone crosstalk between H3S10ph and H4K16ac generates a histone code that mediates transcription elongation. *Cell* **138,** 1122-1136.

Figures

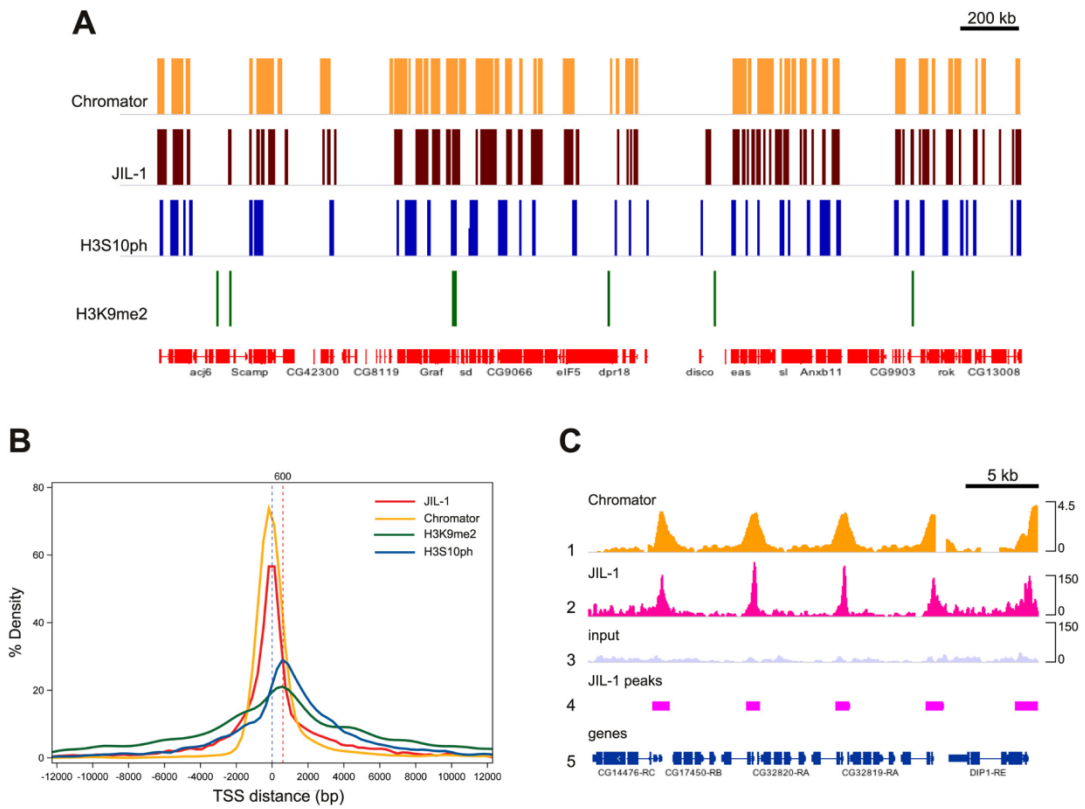

Figure 1. High resolution profiling of JIL-1, H3S10ph, and H3K9me2 enriched genomic regions in *Drosophila* salivary gland cells. (A) Comparison of enriched genomic islands for Chromator (data from ModENCODE), JIL-1 (data from JIL-1(2)), H3S10ph (data from H3S10ph(CS)), and H3K9me2 on a section

of the X chromosome. The location of genes (in red) is indicated below. The enhanced genomic islands were identified using the SICER algorithm (23) with a 200 bp window and a 200 bp gap size. (B) Density of Chromator, JIL-1, H3S10ph, and H3K9me2 enriched islands as determined in (A) plotted relative to the distance from the TSS of nearby genes. Chromator and JIL-1 on average tend to localize to enriched islands with a peak centered near the TSS. H3S10ph and H3K9me2 on average tend to localize with a peak about 600 bp after the TSS. (C) JIL-1 enriched binding peaks strongly correlate with those of Chromator and are preferentially located at the 5'-end of genes. Lane 1, ChIP on chip profile of Chromator (data from ModENCODE). The data is represented as average log2 signal ratio of IP over input. Lane 2, ChIP-Seq profile of JIL-1 (data from JIL-1(2)). The height of the peaks represents the number of reads obtained in each region scaled to the total number of reads. Lane 3, ChIP-Seq input profile. The height of the peaks represents the number of reads obtained in each region scaled to the total number of reads. Lane 4, Peak JIL-1 enriched binding regions determined by the MACS peak finding algorithm (24). Lane 5, the location of genes in the depicted section of the X chromosome.

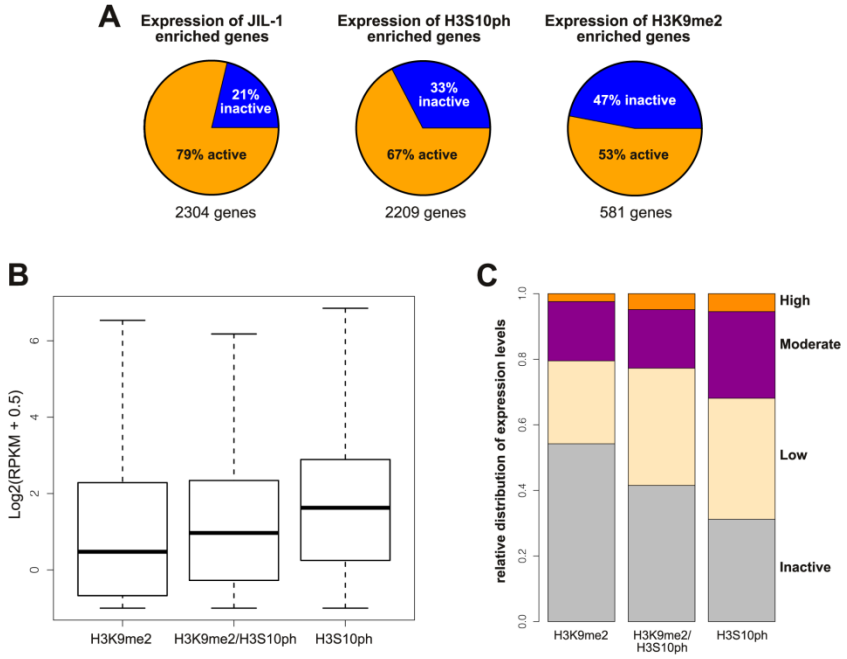

Figure 2. Expression levels of genes enriched for JIL-1, H3S10ph, and/or H3K9me2. (A) Pie charts of the relative proportion of inactive and active (RPKM≥1) genes enriched for JIL-1, H3S10ph, or H3K9me2, respectively. (B) Comparison of the expression of genes enriched for the H3K9me2 or H3S10ph mark only and genes enriched for both marks. Gene expression is represented as log2(RPKM + 0.5). The boxplot representation in this and subsequent figures defines 25th to 75th percentiles (boxes), 50th percentile (lines in boxes), and ranges (whiskers, 1.5 times the interquartile range extended from both ends of

the box or the maximal/minimal value). Outliers were removed from the analysis. The distribution of gene expression for all three categories was significantly different from each other (p-values<0.005; Pairwise Wilcoxon Rank Sum Tests). (C) Stack bar charts showing the distribution of expression of genes enriched for the H3K9me2 or H3S10ph mark only and genes enriched for both marks. Genes with an RPKM of less than one were categorized as inactive whereas active genes were separated into three groups with low, moderate, or high expression levels reflected by RPKMs of from 1-5, >5-30, or >30.

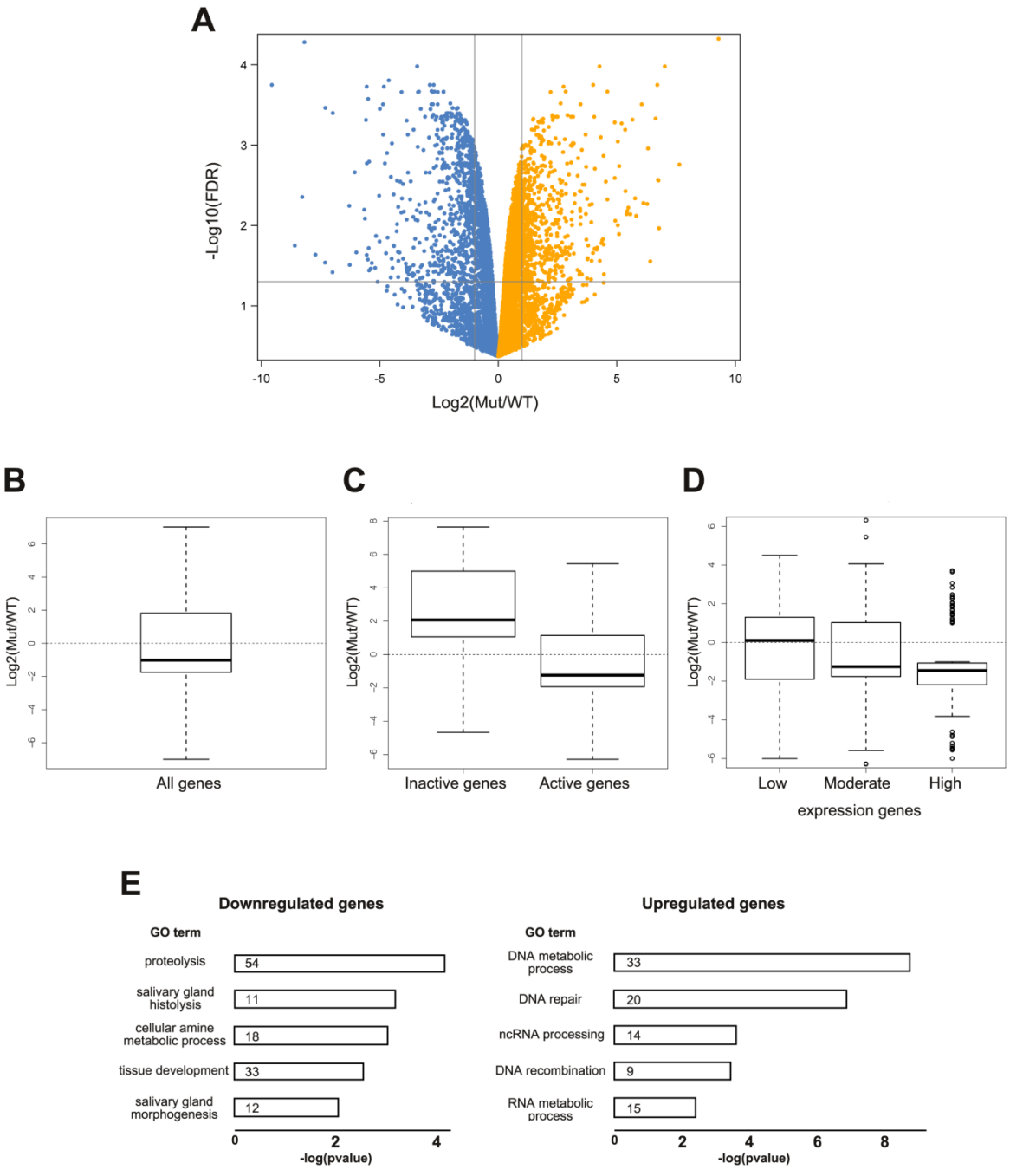

Figure 3. Gene expression can be either down- or upregulated in the absence of H3S10 phosphorylation. (A) Scatter plot of gene expression changes between wild-type and *JIL-1* null mutant salivary gland cells. Negative $\log_{10}$(p-values) from Fisher's exact test were plotted against the $\log_2$(mutant/wild-type) fold change for each gene. Each dot represents a separate gene. Gray lines indicate the cut-offs for 2-fold changes with a FDR equal to 0.05. Downregulated genes in the *JIL-1* mutant are highlighted in light blue and upregulated genes in orange. (B) Box plot of gene expression changes between wild-type and *JIL-1* null mutant salivary gland cells of all genes changed at least 2-fold represented as log2(mutant/wild-type) fold change for each gene. The overall changes in gene expression between the mutant and wild-type were not statistically significant (p-value=0.3, Wilcoxon Signed Rank Test). (C) Box plot of gene expression changes between wild-type and *JIL-1* null mutant salivary gland cells of inactive versus active (RPKM≥1) genes that changed at least 2-fold represented as log2(mutant/wild-type) fold change for each gene. The distribution of gene expression for the two categories was significantly different from each other (p-value<0.0001; Wilcoxon Rank Sum Test). (D) Box plot of gene expression changes between wild-type and *JIL-1* null mutant salivary gland cells of active genes separated into three groups with low, moderate, or high expression levels (RPKMs of from 1-5, >5-30, or >30, respectively) that changed at least 2-fold represented as log2(mutant/wild-type) fold change for each gene. The distribution of gene expression for all three categories was significantly different from each other (low to moderate: p-value<0.01; moderate to high: p-value<0.05; low to high: p-value<0.0001; Pairwise Wilcoxon Rank Sum Tests). (E) Gene Ontology (GO) term of JIL-1 enriched genes identified as down-regulated (left) or up-regulated (right) in *JIL-1* null mutant versus wild-type salivary glands from third instar larvae. The number of genes in each category is shown within the bars. The GO term enrichment was identified by DAVID (32) in Level 5 of biological process, molecular function.

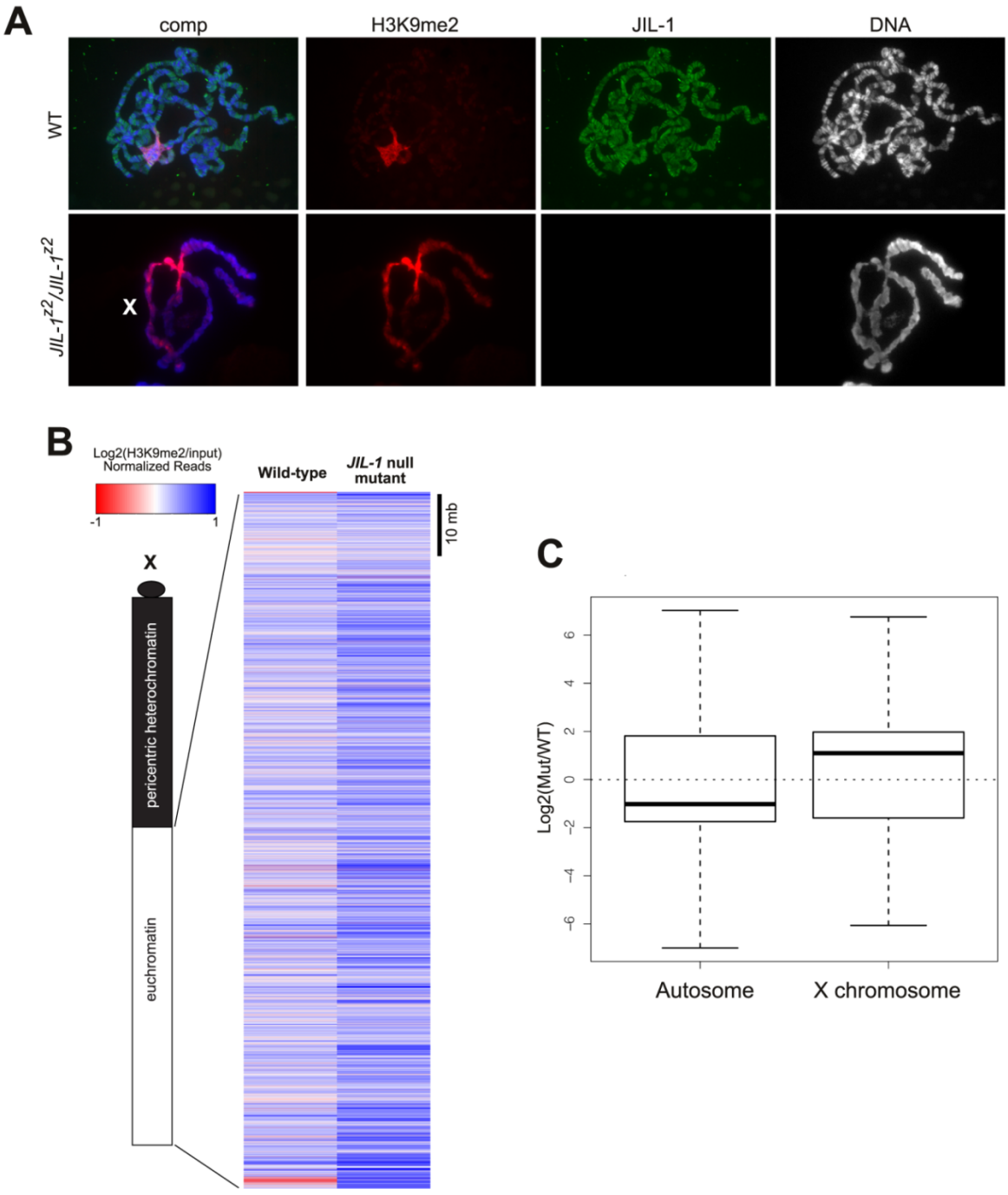

Figure 4. H3K9me2 is redistributed and upregulated on the X-chomosome in *JIL-1* null mutants. **(**A) Wild-type (WT) and *JIL-1* mutant (*JIL-1*^{z2}/*JIL-1*^{z2}) polytene squash preparations labeled with antibody to JIL-1 (in green), H3K9me2 (in red), and with Hoechst (DNA, in blue/gray). The X-chromosome in the *JIL-1* mutant is indicated with an X. (B) Comparison of H3K9me2 distribution in wild-type and *JIL-1* null mutants. The maps show normalized (linear normalization by total library size) read numbers (log2(H3K9me2/input)) in 200 bp bins across the X-chromosome scaled from -1 (dark red) to +1 (dark blue). (C) Box plot of gene

expression changes between wild-type and *JIL-1* null mutant salivary gland cells of autosomal versus X-chromosomal genes that changed at least 2-fold represented as log2(mutant/wild-type) fold change for each gene. The distribution of gene expression for the two categories was similar (p-value=0.4; Wilcoxon Rank Sum Test).

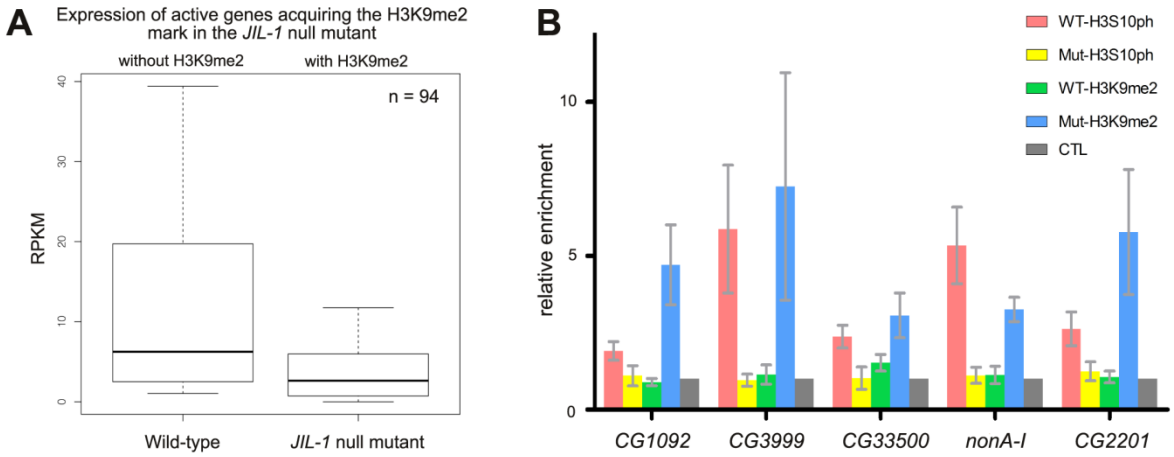

Figure 5. Downregulation of moderate and high expression genes acquiring the H3K9me2 mark in the *JIL-1* null mutant. (A) Box plots of RPKM of active genes (RPKM≥1) in wild-type that acquire the H3K9me2 mark in the *JIL-1* null mutant background. The distribution of gene expression between the two categories was significantly different (p-value<0.0001; Wilcoxon Rank Sum Test). (B) ChIP analysis of randomly selected active genes in wild-type that are downregulated in the *JIL-1* null mutant background. Histograms show the relative enrichment of chromatin immunoprecipitated by anti-H3K9me2 or anti-H3S10ph antibodies from third instar larval salivary glands from wild type (WT) and *JIL-1* null mutant larvae. For each experimental condition the average relative enrichment normalized to the corresponding control immunoprecipitation with anti-GST or anti-IgG antibody from three independent experiments with SD is shown. The difference in H3K9me2 levels for all five genes between wild-type and *JIL-1* null salivary glands was statistically significant (p-values<0.05; two-tailed Student's t-tests).

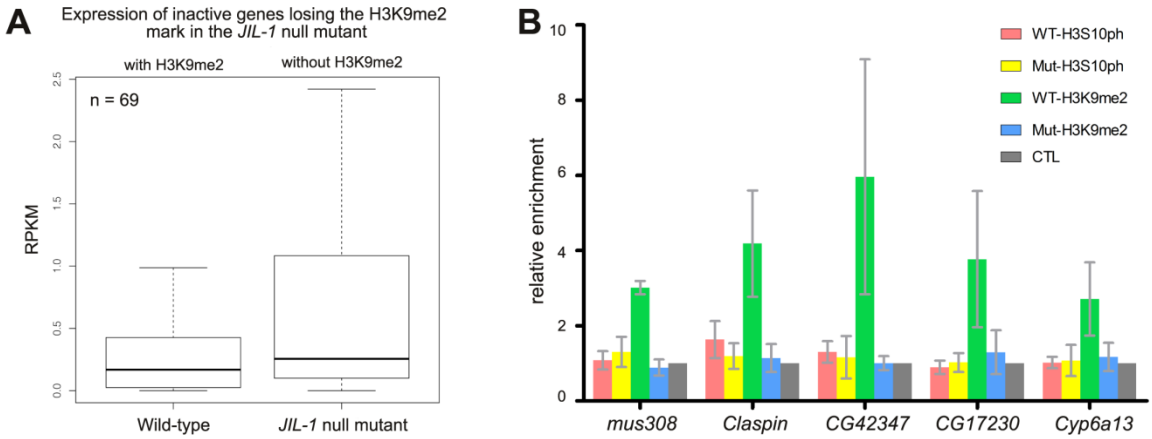

Figure 6. Upregulation of inactive genes losing the H3K9me2 mark in the *JIL-1* null mutant. (A) Box plots of RPKM of inactive genes (RPKM<1) genes in wild-type that lose the H3K9me2 mark in the *JIL-1* null mutant background. The distribution of gene expression between the two categories was significantly different (p-value<0.005; Wilcoxon Rank Sum Test). (B) ChIP analysis of randomly selected inactive genes in wild-type that are upregulated in the *JIL-1* null mutant background. Histograms show the relative enrichment of chromatin immunoprecipitated by anti-H3K9me2 or anti-H3S10ph antibodies from third instar larval salivary glands from wild type (WT) and *JIL-1* null mutant larvae. For each experimental condition the average relative enrichment normalized to the corresponding control immunoprecipitation with anti-GST or anti-IgG antibody from three independent experiments with SD is shown. The difference in H3K9me2 levels for all five genes between wild-type and *JIL-1* null salivary glands was statistically significant (p-values<0.05; two-tailed Student's t-tests).

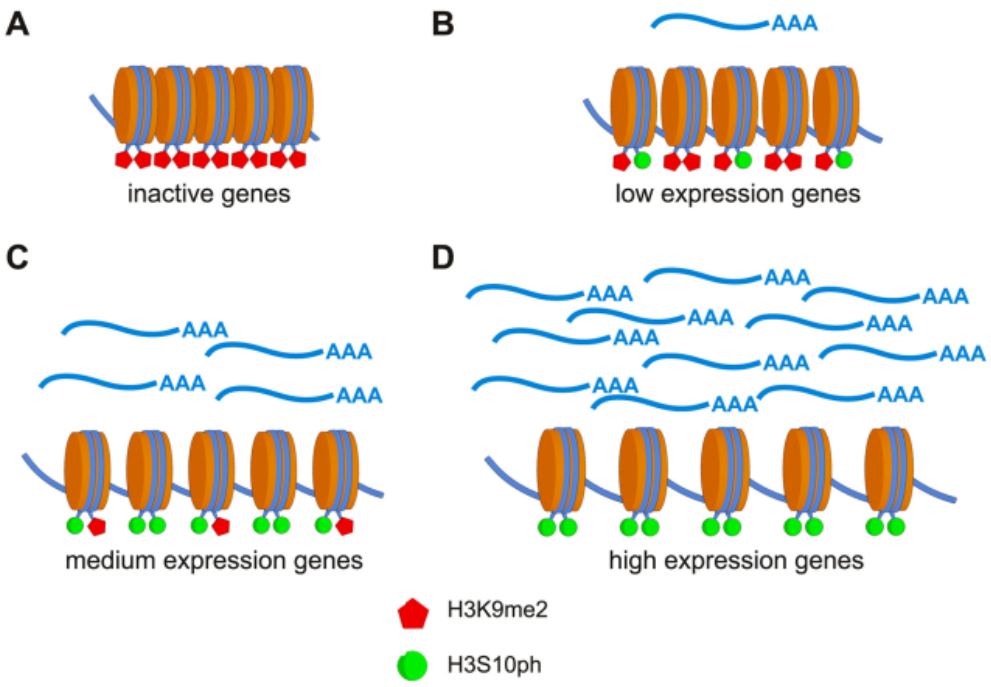

Figure 7. Model for indirect regulation of gene expression by H3S10 phosphorylation. (A) At inactive genes high levels of H3K9 dimethylation lead to a compact chromatin configuration and gene silencing. (B-D) At active genes H3S10 phosphorylation counteracts H3K9 dimethylation leading to a more open chromatin structure facilitating gene expression. In this model gene expression levels are directly correlated with the levels of the H3K9me2 mark independent of the state of the H3S10ph mark, which is not required for either transcription or gene activation to occur.

Supplemental Materials

A

	JIL-1(5c9-1)	JIL-1(5c9-2)	H3S10ph (Active-Motif)	H3S10ph (Cell-Signaling)	H3K9me2 (WT-1)	H3K9me2 (WT-2)	H3K9me2 (*JIL-1Z2*-1)	H3K9me2 (*JIL-1Z2*-2)	Chromator (ModENcode)
JIL-1(5c9-1)	3387								
JIL-1(5c9-2)	2819	5417							
H3S10ph (Active-Motif)	1375	2142	3819						
H3S10ph (Cell-Signaling)	1813	2774	2948	6708					
H3K9me2 (WT-1)	422	709	725	1218	1583				
H3K9me2 (WT-2)	1180	1799	1299	2117	833	3422			
H3K9me2 (*JIL-1Z2*-1)	435	796	624	1047	471	764	1788		
H3K9me2 (*JIL-1Z2*-2)	344	639	432	716	312	694	488	1400	
Chromator (ModENcode)	1746	2229	1056	1335	246	786	359	245	3178

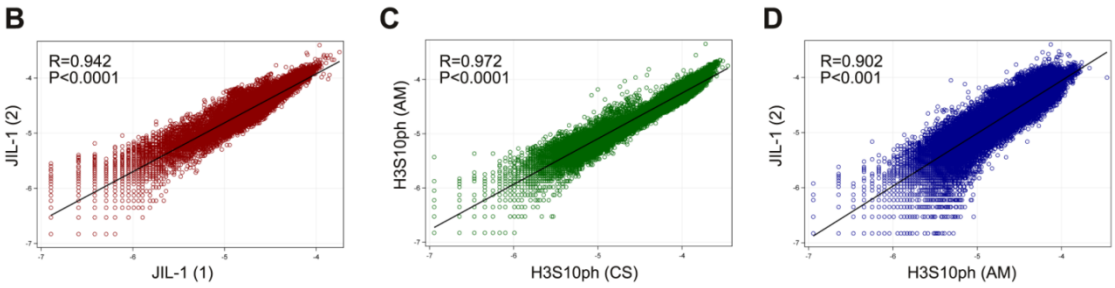

Figure S1. Overview and validation of ChIP-Seq experiments. (A) Table of the number of genes with enriched binding sites for the various modifications determined by ChIP-Seq and the overlap between them. JIL-1(1) and JIL-1(2) represent two independent replications of ChIP-Seq experiments with the JIL-1 mAb 5C9. H3S10ph(AM) and H3S10ph(CS) represent two independent ChIP-Seq experiments with antibodies to H3S10ph from Active Motif and Cell Signaling, respectively. Two sets of independent ChIP-Seq experiments for H3K9me2 were performed with DNA from wild-type (WT-1 and WT-2) and *JIL-1* null (*JIL-1Z2*-1 and *JIL-1Z2*-2) salivary glands using an anti-H3K9me2 mAb from AbCAM. The Chromator data was obtained by ChIP on chip analysis by ModENCODE in Kc cells (25). Enriched genomic islands were identified using SICER (23) and genes with enriched binding or localization sites were annotated using the ChIPpeakAnno R package (26). The number of genes identified by replicated experiments or different antibodies are highlighted in yellow. (B-D) Pair-wise correlation of the JIL-1(1) versus JIL-1(2) (B), H3S10ph(AM) versus H3S10ph(CS) (C), and JIL-1(2) versus H3S10ph(AM) (D) data sets. The number of mapped reads from each data set were determined in 5 kb intervals across the entire genome and each interval was expressed as a proportion of total mapped reads. The data are plotted on a log10 scale and Pearson's coefficient and P-value are indicated on each plot. The data sets were highly correlated validating the results.

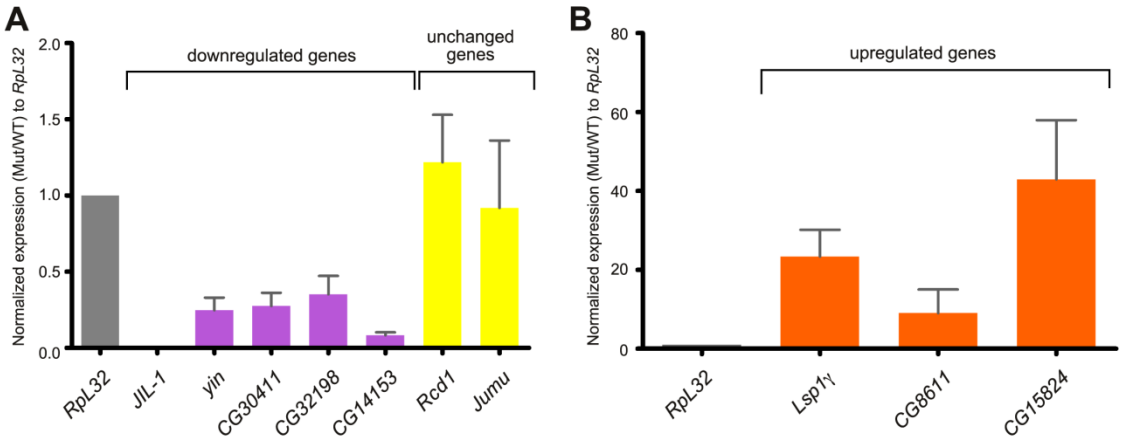

Figure S2. Validation of RNA-Seq experiments. In order to validate the RNA-Seq experiments comparing expression profiles in wild-type and in the *JIL-1* null mutant we performed quantitative PCR (qPCR) experiments on randomly selected genes that were either downregulated, unchanged, or upregulated in the *JIL-1* mutant in the RNA-Seq experiments. A gene's expression was considered down- or upregulated in the mutant if it changed at least two-fold compared to wild-type. In the histograms mutant/wild-type expression for each gene was normalized to the expression of *RpL32* which was unchanged in the *JIL-1* mutant background. For each gene the average normalized expression from three independent experiments with SD is shown. (A) The average expression of all five genes selected based on their downregulation in the *JIL-1* mutant by RNA-Seq were also downregulated at least two-fold as determined by qPCR (in purple). The average expression of two genes selected based on their unchanged status in the *JIL-1* mutant by RNA-Seq were also unchanged as determined by qPCR (in yellow). (B) The average expression of three genes selected based on their upregulation in the *JIL-1* mutant by RNA-Seq were also upregulated at least two-fold as determined by qPCR (in orange).

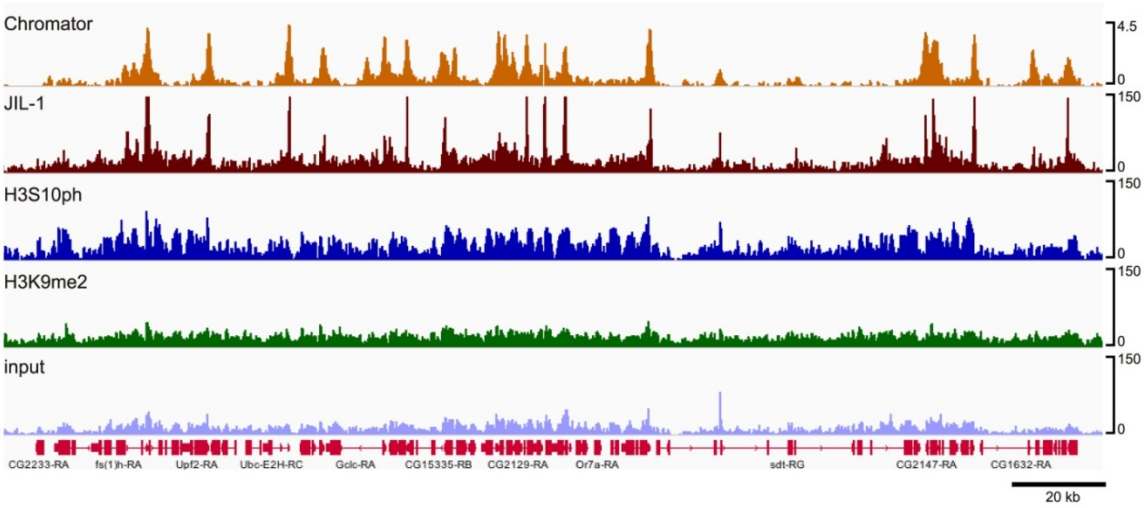

Figure S3. High resolution profiling of JIL-1, H3S10ph, and H3K9me2 genomic sites in *Drosophila* salivary gland cells. ChIP-Seq profiles of JIL-1

(data from JIL-1(2)), H3S10ph (data from H3S10ph(AM)), H3K9me2, and input. The height of the peaks represents the number of reads obtained in each region scaled to the total number of reads. The profile for Chromator shown for comparative purposes is based on ChIP on chip data generated by ModENCODE (25). The data is represented as average log2 signal ratio of IP over input. The location of genes in the depicted section of the X chromosome is shown in red.

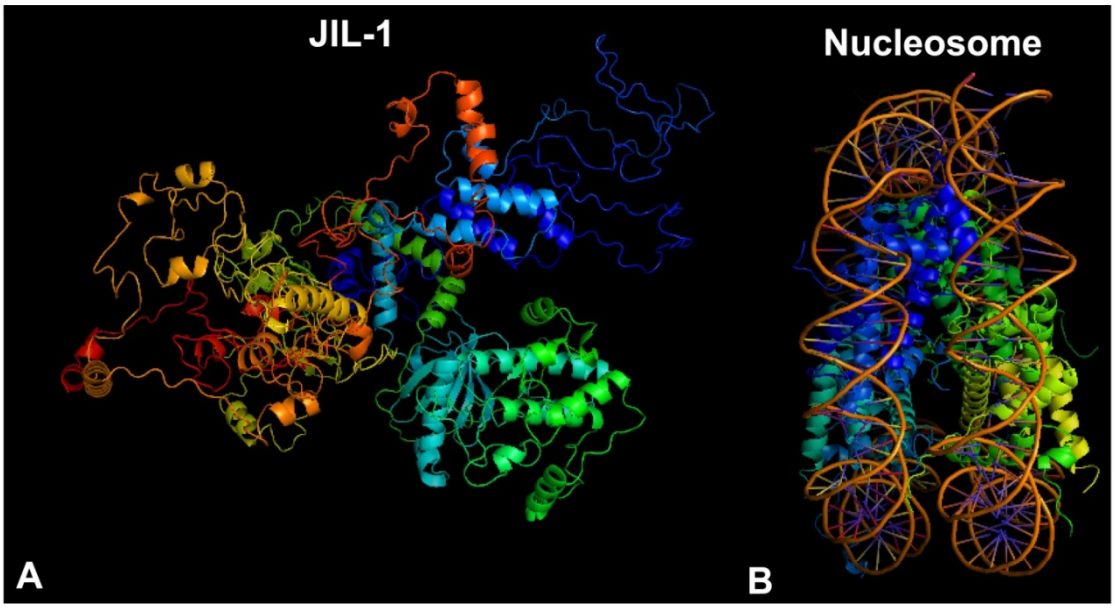

Figure S4. Comparison of the predicted structure of JIL-1 with that of a nucleosome. (A) JIL-1's structure was modeled using the I-TASSER structure prediction platform (37). The amino-terminal domain is rendered in blue, the first kinase domain in green, the second kinase domain in yellow, and the carboxy-terminal domain in red. (B) The crystal structure of a nucleosome (PDB ID: 1AOI). The structures were rendered in PyMOL.

CHAPTER 5. GENERAL CONCLUSION

General Discussion And Future Directions

Domain requirements of JIL-1 for H3S10 phosphorylation and chromatin remodeling

JIL-1 can be naturally divided into four domains, including an NH_2-terminal domain (NTD), two kinase domains (KDI and KDII), and a COOH-terminal domain (CTD) (Jin et al., 1999). JIL-1 CTD was the first characterized domain, and it has been unveiled that it is sufficient for correct chromatin localization, and for the rescue of disturbed chromosome morphology in *JIL-1* null animals (Wang et al., 2011; Deng et al, 2008). In this study, we further characterized other JIL-1 domains, NTD and KDI and II with regards to their function in kinase activity and regulation of chromatin structure. We have shown that a JIL-1 construct without the NTD fails to attain catalytic activity despite the fact that it contains two kinase domains and directs JIL-1 to its proper location in the chromosome. Furthermore, we have illustrated the functions of JIL-1's tandem kinase domains, where mutated phenotypes of either of the two kinase domains is identical to mutating both kinase domains. Additionally, neither JIL-1 "kinase dead" construct is able to phosphorylate H3S10 or rescue disturbed chromosome morphology in *JIL-1* null animals. These observations indicate both kinase domains are required by JIL-1 to attain proper catalytic activity. Additionally, in order to understand the mechanism of kinase domain activation we have studied phosphorylation sites on JIL-1, as the catalytic activity of its homolog MSK1 is regulated via multisite phosphorylation by upstream kinases and auto-phosphorylation. We have

detected that JIL-1 is phosphorylated at Ser^{424}, which is conserved in MSK1. Mutation of this site leads to loss of JIL-1's kinase activity.

For further study, one direction is to identify the crystal structure of JIL-1 or each of its domains, which will dramatically advance our understanding of the mechanism of JIL-1's interaction with chromatin.

Genome-wide study of JIL-1 and its mediated H3S10 phosphorylation in regulating gene expression via coordinating the distribution of gene silencing mark

It has been demonstrated in previous studies using genetic interaction assays and position-effect variegation assays that JIL-1 is capable of counteracting the gene silencing effect of heterochromatin markers H3K9me2, Su(var)3-7 and HP1a (Zhang et al., 2006; Deng et al., 2007; Deng et al., 2010; Wang et al., 2011). In addition, by studying the reporter *white* gene, we have further shown that the levels of H3K9 dimethylation at this locus inversely correlates with its level of expression, and that H3K9 dimethylation levels in turn are regulated by H3S10 phosphorylation (Wang et. al., 2012). In order to understand the genome-wide interplay between JIL-1-mediated H3S10 phosphorylation and gene silencing marker H3K9 dimethylation in terms of regulating gene expression and chromatin structure, we conducted a genome-wide analysis of protein distribution profiles and transcription profiles.

In this study we have examined the genome-wide distribution of JIL-1, H3S10 phosphorylation, and H3K9 dimethylation marker using ChIP-seq. The distribution profiles have identified that JIL-1's binding peaks are located closely to transcription start sites (TSS) whereas peaks of H3S10 phosphorylation and H3K9 dimethylation are 600 base pairs downstream of the TSS and much

broader. Furthermore, combining the distribution data with the transcription profile attained from RNA-seq, we also confirm that JIL-1 and H3S10 phosphorylation are predominantly enriched at active genes, whereas more than half of the gene-silencing marker H3K9 dimethylation is localized at inactive genes. Then, by comparing transcription profiles from wild type and *JIL-1* null animals, we have found that approximately 1500 genes change at least 2-fold in expression level, where most of the activated genes in the JIL-1 mutant are originally repressed in wild type animals and most the of inactivated genes are originally activated. In addition, we have discovered that in the absence of H3S10 phosphorylation, loss of H3K9 dimethylation correlates with activation of silent genes and gain of H3K9 dimethylation correlates with repression of active genes.

In summation, these results support a model where gene expression levels are regulated by the levels of H3K9 dimethylation, and H3S10 phosphorylation is able to indirectly maintain active transcription by counteracting H3K9 dimethylation.

One of the future directions is closely related to the previous project's future direction, which is to identify the crystal structure of JIL-1. Based on ChIP-seq data and 3D structure prediction, there is an approximately a 600 base pair gap between the binding sites of JIL-1 and H3S10 phosphorylation. It would very helpful to learn the interaction between them via studying the protein structure. Another direction is to study relationships between JIL-1 and other chromatin proteins using publicly available next-generation sequencing data, such as from modENCODE. By comparing different protein distribution and transcription

profiles with newly developed algorithms, it is possible to discover interesting biological findings.

References

Deng H, Bao X, Zhang W, Girton J, Johansen J and Johansen KM. (2007). Reduced levels of Su(var)3-9 but not Su(var)2-5 (HP1) counteract the effects on chromatin structure and viability in loss-of-function mutants of the JIL-1 histone H3S10 kinase. *Genetics* 177 : 79-87.

Deng H, Bao X, Cai W, Blacketer MJ, Belmont AS, Girton J, Johansen J and Johansen KM. (2008). Ectopic histone H3S10 phosphorylation causes chromatin structure remodeling in *Drosophila*. *Development.* 135 : 699-705.

Deng H, Cai W, Wang C, Lerach S, Delattre M, Girton J, Johansen J and Johansen KM. (2010). *JIL-1* and *Su(var)3-7* interact genetically and counterbalance each others' effect on position effect variegation in *Drosophila*. *Genetics* 185 : 1183-1192.

Wang C, Cai W, Deng H, Bao X, Girton J, Johansen J and Johansen KM. (2011). The epigenetic H3S10ph mark is required for counteracting heterochromatic spreading and gene silencing in *Drosophila*. *J. Cell Sci.* 124 : 4309-4317.

Wang, C., W. Cai, Y. Li, J. Girton, J. Johansen and K.M. Johansen. (2012). H3S10 phosphorylation by the JIL-1 kinase regulates H3K9 dimethylation and gene expression at the *white* locus in *Drosophila*. *Fly* 6 : 93-97.

Zhang W, Deng H, Bao X, Lerach S, Girton J, Johansen J and Johansen KM. (2006). The JIL-1 histone H3S10 kinase regulates dimethyl histone H3K9 modifications and heterochromatic spreading in *Drosophila*. *Development* 133 : 229-235.

ACKNOWLEDGEMENTS

The entire work is supported by National Institutes of Health (NIH) Grant GM62916. This research was performed at the Roy J. Carver Department of Biochemistry, Biophysics & Molecular Biology.

I would foremost like to thank Dr. Kristen Johansen and Dr. Jørgen Johansen for giving me the pleasure to join their lab. Science is never easy; when I had issues with my research, they were always there with advice and encouragement. During my PhD, they have taught me how to think like a real scientist, and my English has largely improved due to Jørgen's kindly and persisting critiques. Second, I would like to thank Dr. Jack Girton for leading me to the magic world of Genetics, and giving me precious advice on solving difficult genetic issues. Without his generous help, I wouldn't have been able to implement many of my experiment plans. Third, I would like to thank Dr. Weili Cai and Dr. Changfu Yao for teaching me everything they could about our instruments and techniques, and especially Weili for collaborating me on the JIL-1 NTD paper. Their mentoring and advice has been invaluable during my PhD.

I would like to thank the Johansen group members for their friendship, including Dr. Chao Wang and Saheli Sengupta. They are always of great help whether it is technical advice or interesting discussions. I would also like to thank my committee members for their assistance, Dr. Hui-Hsien Chou and Dr. Edward Yu.

I would like to thank the many friends I have made since I moved to Ames from China. They made this time extremely enriching and enjoyable. I would like to thank my parents Guixin Li and Tiantao Li for their love and support. Last, I

would like to thank my husband Dr. Timothy Anderson for his love and support with my career, while allowing me to have two lovely birds, Morgan and Tesla. You are not the reason why I came to ISU, but it turns out you are best thing that happened to me at ISU!